4. EXPERIMENTAL INVESTIGATION OF THE BOUNDARY LAYER PROPERTIES

The aims of the work presented in this section were to establish the mean properties of the thick turbulent axisymmetric boundary layer generated on a long slender cylinder in axial flow, and thus to examine the effect of transverse curvature in producing deviations of the boundary layer properties from the flat plate case. Evidence for turbulent flow mechanisms resulting from the transverse curvature has been examined in the relationship between the inner and outer boundary layer regions. The divergence of the boundary layer properties from the axisymmetric case at small yaw angles has been examined.

Preliminary investigations were conducted to establish the flow regime where the axisymmetric boundary layer is turbulent, and to determine the boundary between the essentially attached boundary layer flows at small angles of yaw, and the separating flow regimes associated with vortex shedding at larger yaw angles.

The most appropriate form of the normalising length scale which leads to similarity of different boundary layer velocity profiles has been determined, and the effects of transverse curvature on the inner-layer properties scaled on wall units have been examined.

4.1 The Long Slender Cylinder in Axial Flow

Initial measurements of the velocity within the boundary layer generated on a long slender cylinder in axial flow were made in order to determine the flow conditions and the cylinder geometry for which a thick turbulent axisymmetric boundary layer could be generated by a cylinder aligned within the test section of the low-speed wind-tunnel. The fluctuating velocity within the boundary layer was examined using an oscilloscope to display the output from a hot-wire probe as the probe was traversed across the boundary layer from near the cylinder surface at y = 0.1 mm, to the approximate outer edge of the boundary layer at y = 30 mm. The free stream velocity at which the boundary layer was fully turbulent was then recorded for different cylinder diameters and streamwise locations.

The results of these measurements are shown in Figure [4.1], and an approximate boundary for fully turbulent boundary layers as a function of the cylinder Reynolds number $Re_a = U_1 a/\nu$ and streamwise location x/a has been determined. These results indicate that an investigation of fully turbulent thick axisymmetric boundary layers may be conducted in the low-speed wind-tunnel using 0.9-mm-diameter cylinders for Reynolds numbers above $Re_a = 250$ at a streamwise location x = 2.7 m (x/a = 6000) downstream of the entry to the test section. These measurements, and the subsequent investigations, were all conducted with the side walls of the wind-tunnel test-section adjusted to maintain a uniform free stream velocity along the test-section with the test cylinder in place, and with the upstream end of the cylinder located at the start of the test section (x = 0). The boundary-layer momentum thicknesses corresponding to the chosen flow conditions are in the range $2000 < Re_{\theta 2} < 3000$.

For the cylinder radius chosen for this investigation (a = 0.45 mm), the Reynolds number limit for fully turbulent boundary layers was also determined at a single streamwise position at the end of the test section with the test section side walls parallel. This measurement, shown in Figure [4.1], suggests that the small variations in pressure gradient resulting from the generation of boundary layers on the test section walls (in the parallel configuration) do not have any significant effect on the limits for fully turbulent boundary layers in the current experimental configuration.

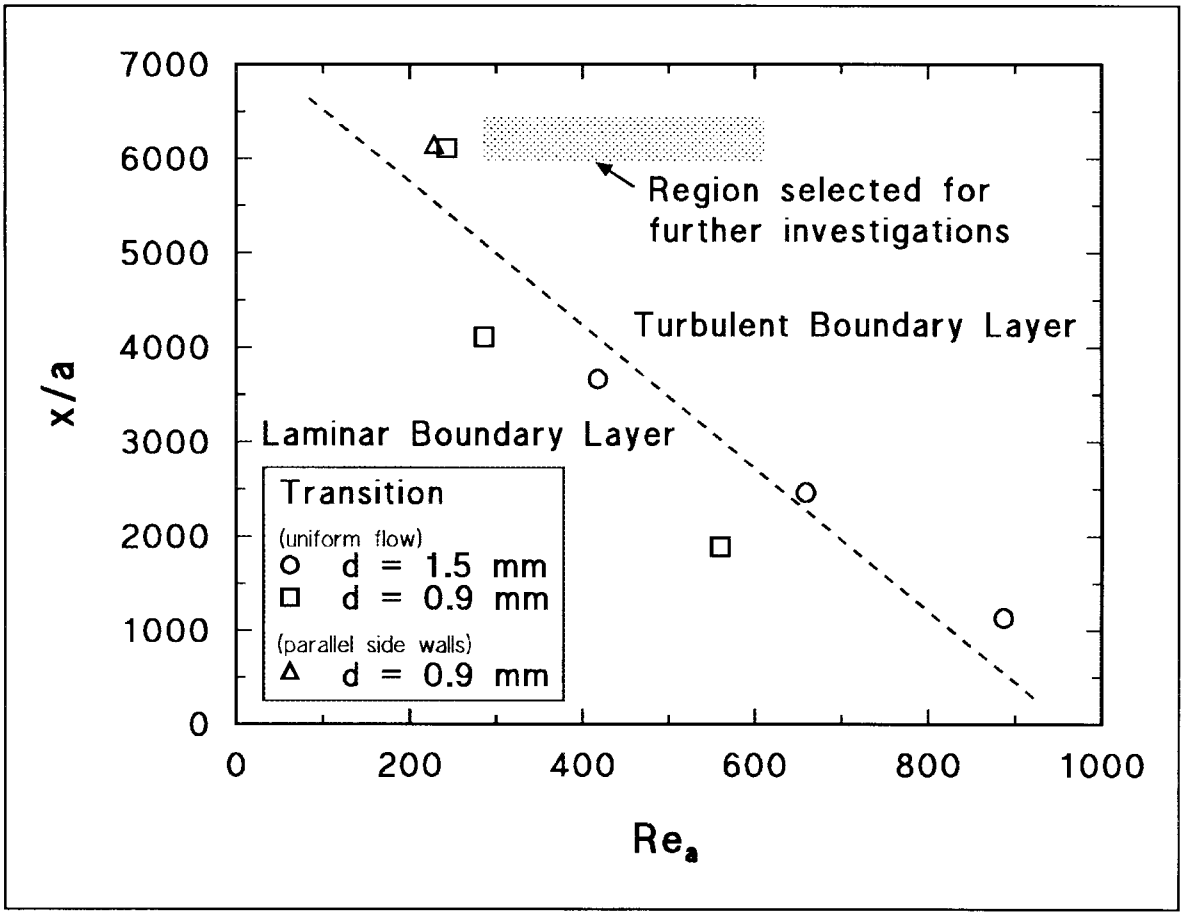

Figure 4.1 Measurement of the lower limit of Reynolds number Re_a for which the axisymmetric boundary layer is fully turbulent at different streamwise locations x/a for different cylinder diameters d. The flow regimes selected for further investigation of the turbulent boundary layer are indicated as a shaded region.

The current investigation of the boundary layers generated on long slender cylinders in axial flow is restricted to cases where the effect of transverse curvature should be most apparent. Previous investigations (Willmarth et.al.1976; Luxton et.al.1984) have indicated that such cases occur for large δ/a and small a+ which may be achieved by large x/a and small Re_a. The current investigations, for which the ratios of cylinder radius to outer length scale a/δ and to inner length scale $aU_\tau/\nu = a_+$ are shown in Figure [4.2], were conducted at as large a ratio x/a as practicable in the available test facility, and for different small values of Re_a for which the boundary layer is fully turbulent.

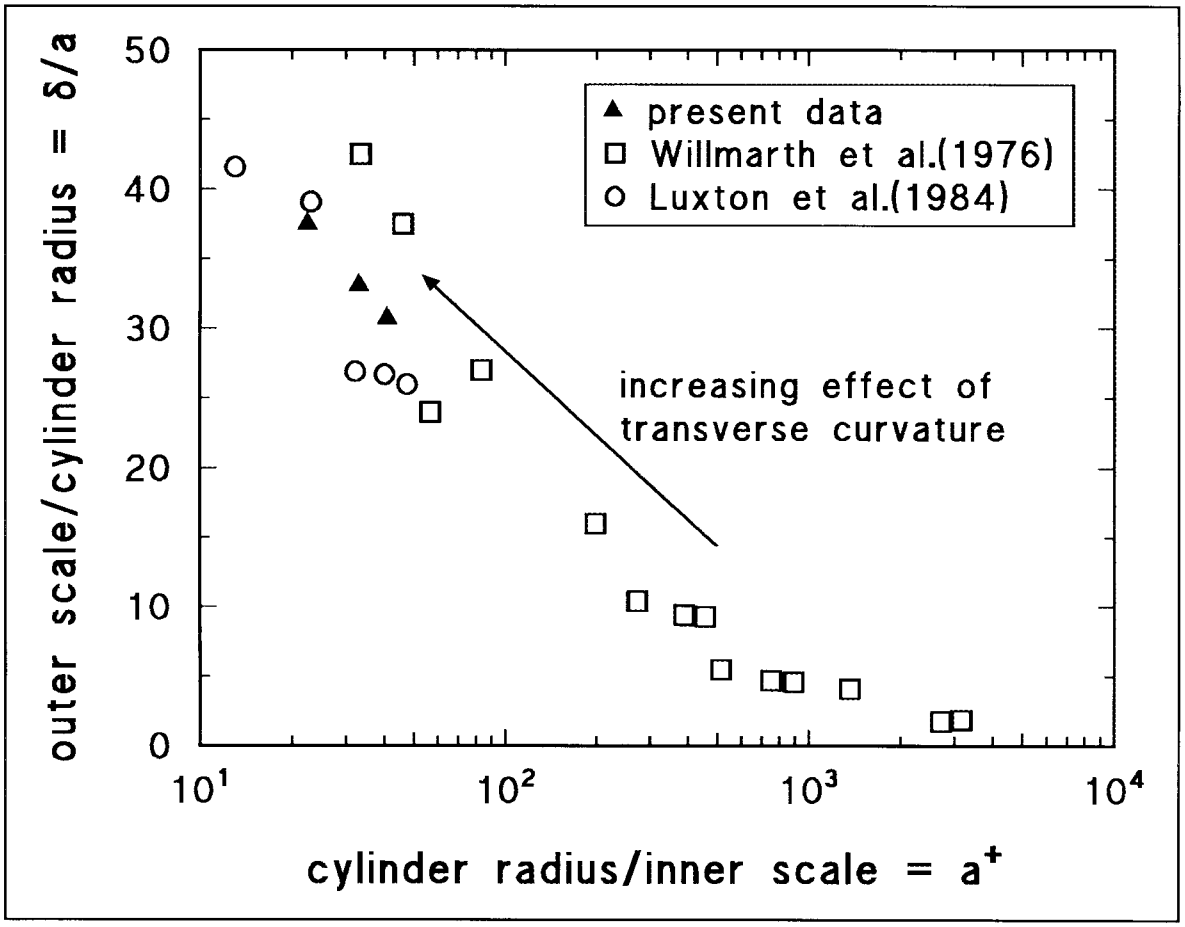

Figure 4.2 The current investigation of thick axisymmetric turbulent boundary layers within the region determined by previous investigators where the effects of transverse curvature are significant.

4.1.1 Mean properties of the axisymmetric boundary layer

The mean velocity in the boundary layer was measured by the calibrated DC voltage output (with a time constant of three seconds) of the hot wire anemometer using a small Wollaston wire probe. Measurements were made throughout the boundary layer thickness for Reynolds numbers Re_a = 300, 450 and 600 at distances measured from the cylinder surface from y = 0.05 mm to y = 30 mm.

The accuracy of the measurement of y close to the cylinder surface was improved from that obtained using the optical positioning method by using two hotwire probes mounted on the same micrometer traverse approximately 100 mm vertically apart, with one probe above the cylinder and the other below. By measuring the distance traversed between positions of equal velocity close to the surface on opposite sides of the axially aligned cylinder it was possible to resolve the location of the cylinder surface at the resolution of the micrometer traverse (0.01 mm).

The comparison of measurements made close to the cylinder surface using hotwire probes of different active length, and measurements made using a miniature pitot tube (Luxton et.al.1984), indicated that the hotwire probe measurements were affected by the transverse curvature of the cylinder surface, which results in the ends of the active length of the hot-wire being further away from the cylinder surface than the centre region. As the distance y is measured between the centre of the probe active length and the cylinder surface, the average velocity over the sensor corresponds to a slightly larger value of y.

From these experimental measurements a correction formula has been obtained for the distance y corresponding to the location of the average velocity measurement, as a function of the cylinder radius a, the probe active length l, and the measured distance between the cylinder surface and the centre of the hotwire probe active length y′:

$$y = \sqrt{\{(y'+a)^2+(l/4)^2\}} - a \qquad [4.1]$$

All of the measurements made in the cylinder boundary layer were corrected for transverse curvature effects using Equation [4.1], and the hotwire probe design with the smallest available active length (0.3 mm) was used for all subsequent velocity measurements except where noted otherwise. For the small probes used here the largest correction to the measurement of y, at the point closest to the surface, was an increase of 0.0056 mm which is of the same order as the accuracy of the original measurement of y based on the resolution of the probe positioning traverse.

For quantitative consideration of the effects of transverse curvature on the mean-velocity profile, length and velocity scales characterising the wall region and the outer region of the boundary layer are required. For the outer layer, the boundary layer thickness δ or a related integral scale and the free-stream velocity U_1 are the appropriate scales; for the inner layer, the relevant scales are the wall scales ν/U_τ and U_τ, determined by the wall shear stress τ_w and the fluid viscosity ν, where U_τ is the friction velocity given by $U_\tau = \sqrt{(\tau_w/\rho)}$.

The choice of outer-layer length scale is based on the following considerations. The general characteristic of the measured mean velocity profiles across the boundary layer thickness is that the profiles are very "full", that is, there is a rapid increase in velocity through the inner region and a very gradual increase in velocity throughout the

outer region, giving approximately 90% of the velocity increase in the inner 10% of the boundary layer. As the remaining 10% of the velocity increase is spread over 90% of the boundary layer the estimation of the boundary layer thickness δ at $U/U_1 = 0.99$ will be of limited accuracy and thus δ is not well suited for use as a characteristic outer-layer length scale to normalise the measured y values.

Values of δ have been estimated by linear interpolation between consecutive velocity measurements which span the 99% free stream velocity location. From the measured velocity distributions at x/a =6000 the estimates of boundary layer thickness δ are 16.9, 14.9 and 13.8 mm at Re_a = 300, 450 and 600 respectively, giving corresponding ratios δ/a of 38, 33 and 31 which have been used in Figure [4.2] to indicate the general nature of these boundary layers.

A more reliable method of normalising the velocity profile data is to use an integral length scale such as the displacement thickness δ^*, or the momentum thickness θ which may be calculated as for a flat-plate boundary layer as:

$$\delta^* = \int_0^{\delta} \left[1 - \frac{U}{U_1}\right] dy \qquad [4.2]$$

$$\theta = \int_0^{\delta} \frac{U}{U_1}\left[1 - \frac{U}{U_1}\right] dy \qquad [4.3]$$

and the shape factor

$$H = \frac{\delta^*}{\theta} \quad . \qquad [4.4]$$

The measured velocity profiles are shown in Figure [4.3] as U/U_1 versus y/θ for the three Reynolds numbers, and the inner region of the boundary layer is shown to a

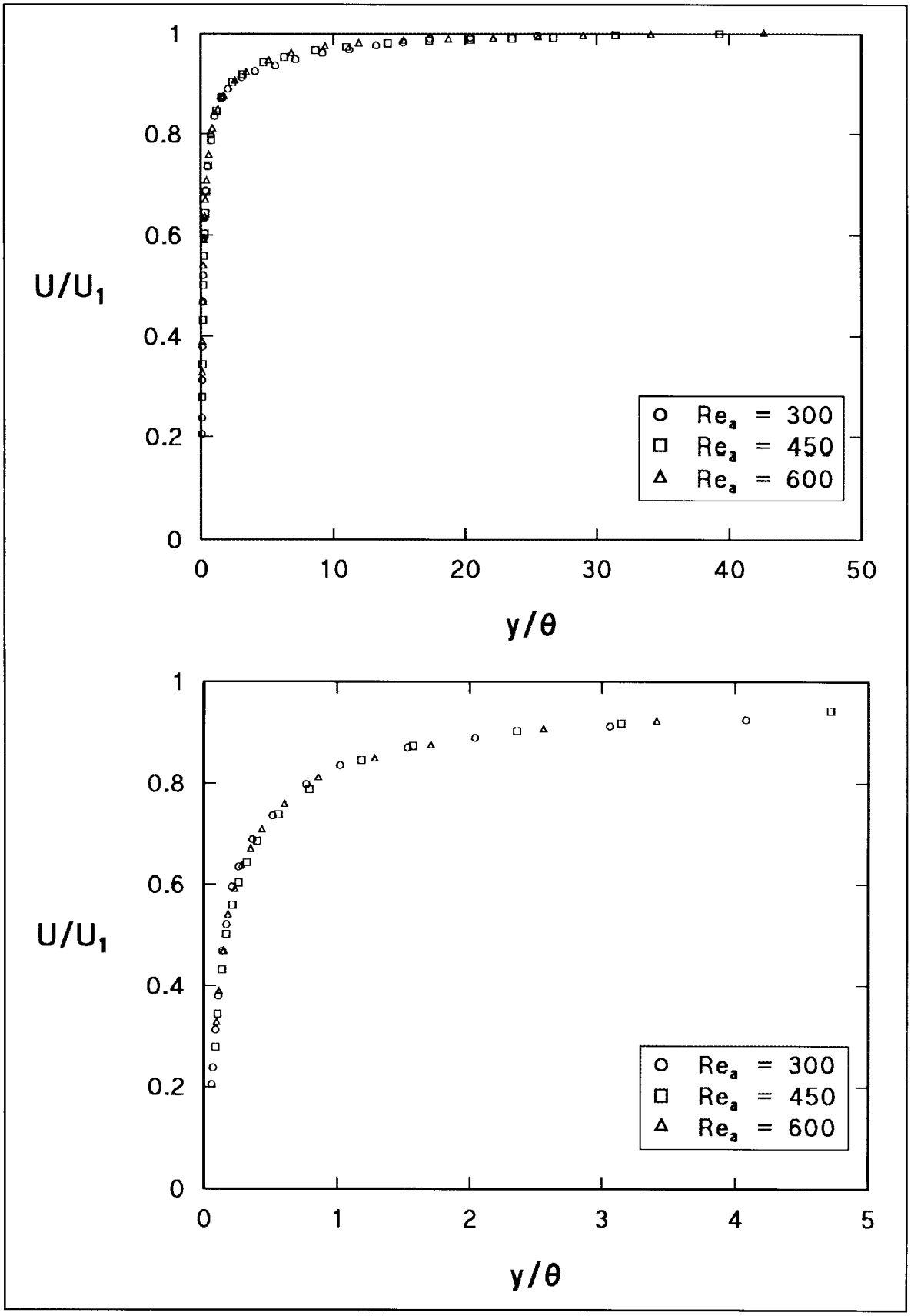

Figure 4.3 Mean velocity distribution in the boundary layer with y/θ.

Lower graph is the inner region expanded to a larger scale.

larger scale for clarity in the lower graph. The collapse of the three sets of data to a single curve in the non-dimensional form indicates that the flat-plate boundary layer momentum thickness is an adequate length scale for the thick axisymmetric turbulent boundary layers generated on long slender cylinders in axial flow, at least for the relatively narrow range of Re_a, Re_x and δ/a for which the current experiments have been conducted. However, for comparing data for boundary layers covering a significantly larger range of δ/a values, a more generally applicable integral length scale incorporating the curvature of the cylinder surface should be used. Two different definitions for both the displacement thickness and the momentum thickness for axisymmetric boundary layers have been produced by previous researchers, and both remain in common use today. In order to avoid the possibility of confusion in the interpretation of results that two such definitions might cause, Glauert and Lighthill (1955) make use of the displacement area Δ and the momentum defect area Θ which are common to both sets of definitions, given by

$$\Delta = \int_{a}^{a+\delta} \left[1-\frac{U}{U_1}\right] 2\pi r \, dr \qquad [4.5]$$

and

$$\Theta = \int_{a}^{a+\delta} \frac{U}{U_1}\left[1-\frac{U}{U_1}\right] 2\pi r \, dr \quad . \qquad [4.6]$$

Length scales (thicknesses) may then be obtained, as for a flat plate, by dividing each area by the length/circumference of the solid surface ($2\pi a$) giving

$$\delta_1^* = \int_{a}^{a+\delta} \left[1-\frac{U}{U_1}\right] \frac{r}{a} \, dr \qquad [4.7]$$

and

$$\theta_1 = \int_a^{a+\delta} \frac{U}{U_1}\left[1-\frac{U}{U_1}\right]\frac{r}{a}\,dr \quad , \qquad [4.8]$$

and

$$H_1 = \frac{\delta_1^*}{\theta_1} \quad . \qquad [4.9]$$

The equation for displacement thickness δ_1^* [4.7] is given by Seban and Bond (1951), and the equation for momentum thickness θ_1 [4.8] by Eckert (1952).

Alternatively, the length scales may be obtained by considering, as for a flat plate, the outward displacement of the surface represented by each area, giving

$$(\delta_2^* + a)^2 - a^2 = \int_a^{a+\delta} \left[1-\frac{U}{U_1}\right] 2r\,dr \quad , \qquad [4.10]$$

$$(\theta_2 + a)^2 - a^2 = \int_a^{a+\delta} \frac{U}{U_1}\left[1-\frac{U}{U_1}\right] 2r\,dr \quad , \qquad [4.11]$$

and

$$H_2 = \frac{\delta_2^*(1+\frac{\delta_2^*}{2a})}{\theta_2(1+\frac{\theta_2}{2a})} \quad . \qquad [4.12]$$

The equation for displacement thickness δ^*_2 [4.10] is given by Kelly (1954), and the equation for momentum thickness θ_2 [4.11] by Richmond (1957). The alternative definitions are shown diagrammatically in Figure [4.4]. When the boundary layer thickness is smaller than or of the same order as the cylinder radius, the two definitions

yield similar results; however, when the boundary layer thickness is significantly larger than the cylinder radius ($\delta >> a$) the first set of definitions give very large values relative to the boundary layer thickness δ because they do not represent a radial distance from the cylinder surface. Thus while δ_1^* and θ_1 are valid length scales, they do not correspond to a "thickness" of the axisymmetric boundary layer. δ_2^* and θ_2 are therefore the most appropriate length scales.

Values for all three definitions of displacement thickness, momentum thickness and shape factor, calculated for the Reynolds number range covered by the current investigation, are shown in Figure [4.5]. The relative magnitudes of the thickness values are in agreement with previous research (Patel et.al.1974, Luxton et.al.1984), and all three parameters approach constant values as the Reynolds number increases. Thus, at the higher Reynolds numbers the selection of any particular definition of the integral lengths for use as a normalising length scale is not critical, but at the lower Reynolds numbers, where the effects of transverse curvature are the greatest, δ^*_2 or θ_2 is the most appropriate scale.

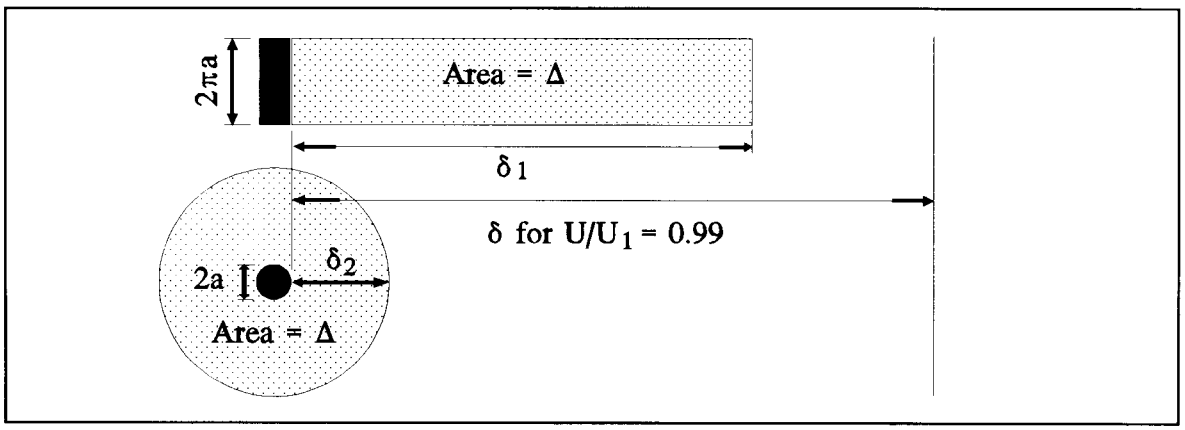

Figure 4.4 Definitions of displacement thickness in terms of the displacement area.

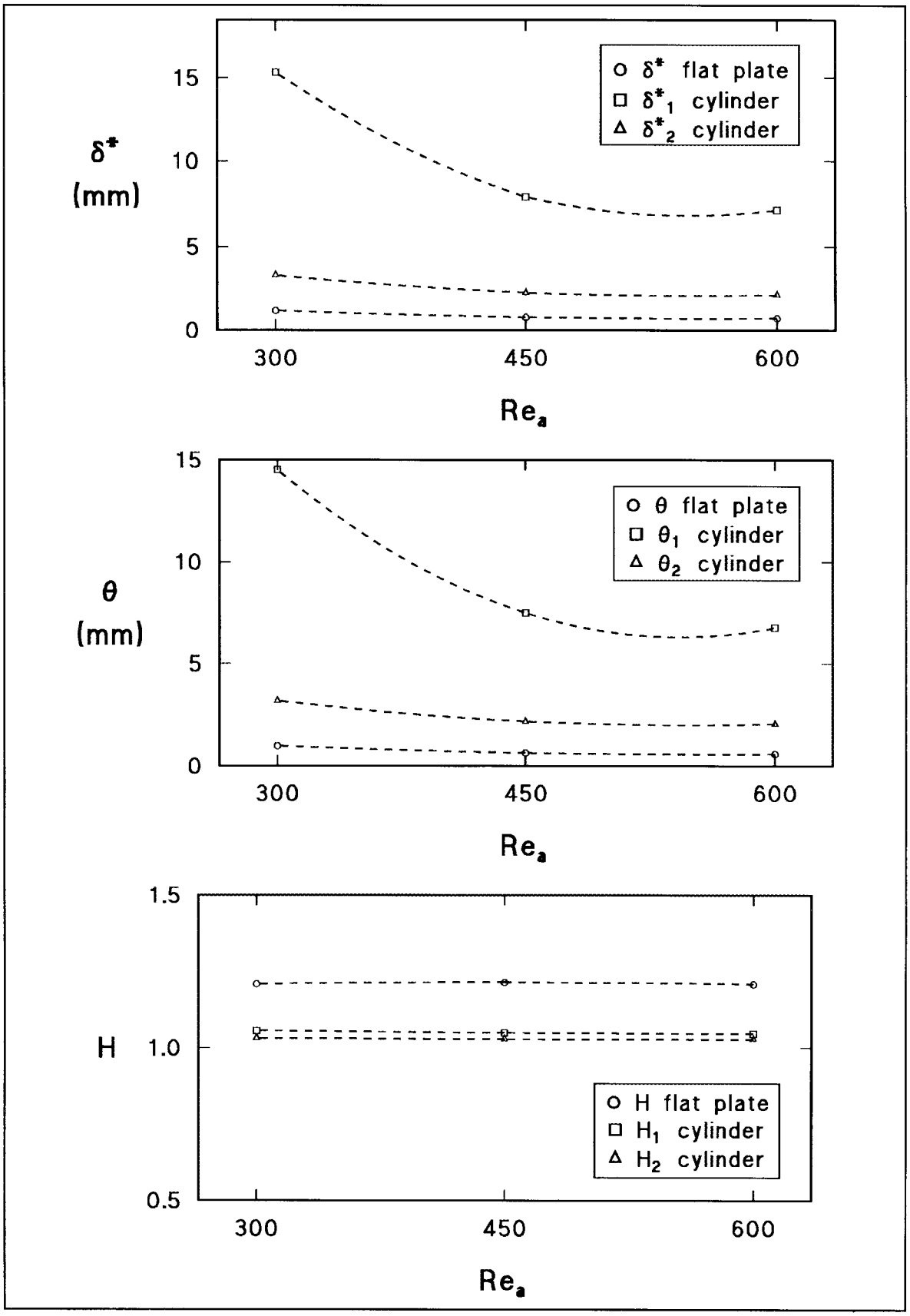

Figure 4.5 The influence of Re_a on the different definitions of δ^*, θ and H.

In the examination of the velocity profiles (Figure [4.3]), the flat-plate momentum thickness θ has been used, primarily for accuracy of calculation. Compared with the flat-plate integral, the r/a weighting of the intergrand in the axisymmetric integrals amplifies the effect of even small variations in mean velocity in the outer region of the boundary layer. As a result, the accuracy of calculation of the axisymmetric integral scales is just as dependent on the last few outer-layer measurements as is the determination of the boundary layer thickness at $U/U_1 = 0.99$.

The similarity of the velocity profiles in the inner region (lower graph, Figure [4.3]) based on an integral length scale (an outer region scale) suggests that either the entire boundary layer is controlled to a large extent by the outer flow, or that the integral length scale is dominated by effects in the inner region. The velocity profiles with the radial position normalised on the axisymmetric momentum thickness θ_2 are shown in Figure [4.6]. They also indicate similarity of the boundary layer in the inner region in terms of scaling on an outer-region length. The inclusion of the effect of transverse curvature in the calculation of θ_2 (and the consequent dominance of the outer-region velocity variation in determining θ_2) discounts the possibility that inner-region similarity in terms of an outer-region length is simply the effect of an inappropriate length scale. This adds weight to the proposition that the inner region is, to a large extent, controlled by outer flow variables.

A comparison of the present data with previous results by Willmarth et.al.(1976) for a value of δ/a similar to that for the current data, and also for a smaller value of δ/a, is shown in Figure [4.6]. The difference between the current results and

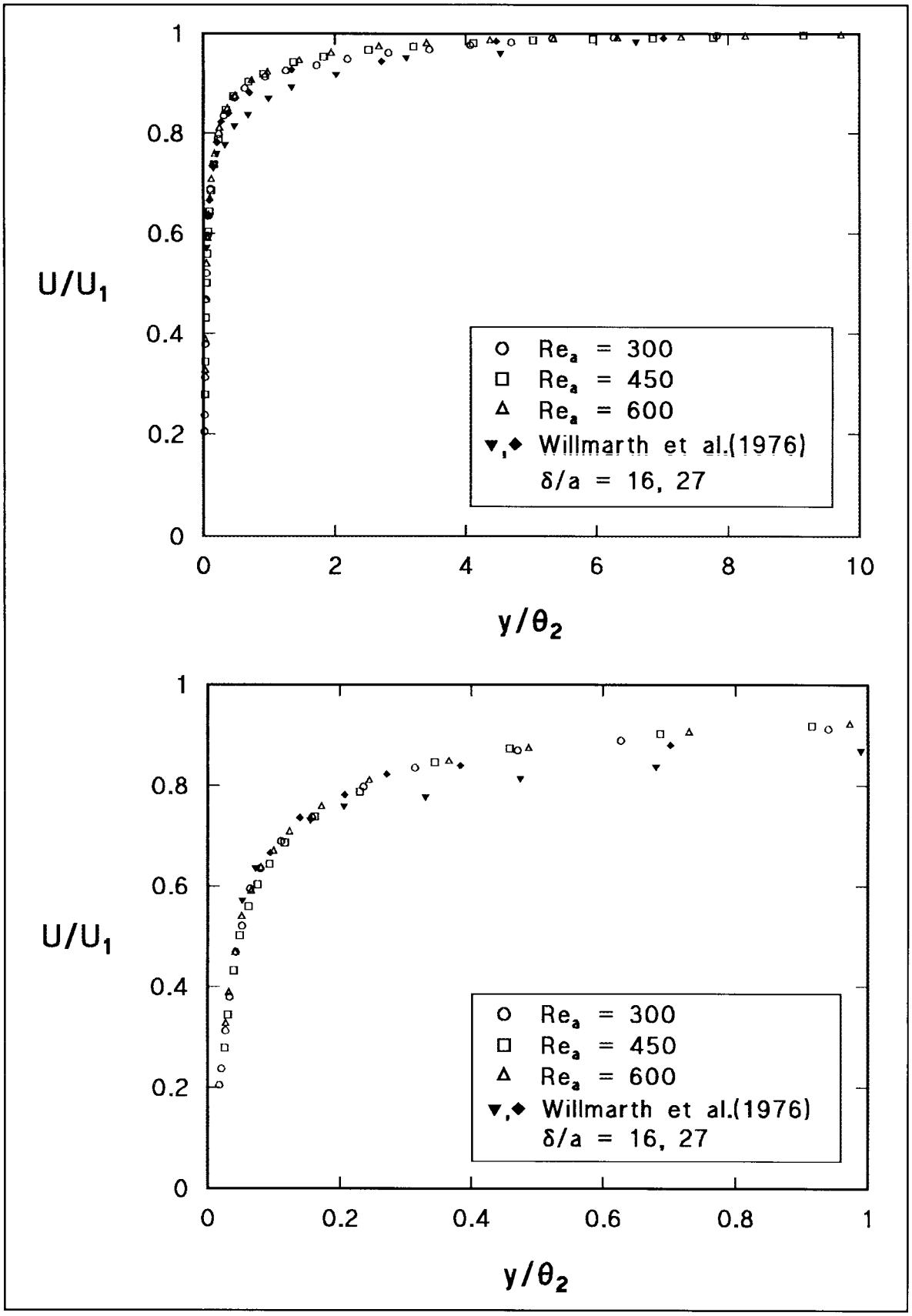

Figure 4.6 Mean velocity distribution in the boundary layer with y/θ_2.

Lower graph is the inner region expanded to a larger scale.

Willmarth's data at small δ/a suggests that there is no overall similarity based on the integral momentum thickness for axisymmetric boundary layers over a large range of δ/a. The similarity shown between the current data and those of Willmarth for δ/a of similar magnitude but at much larger Reynolds number (Re_a = 1,439) suggests that in the region where δ/a is large, similarity extends over a large range of Reynolds numbers.

The existence of similarity of flow based on an outer-region length scale, over a range of Reynolds numbers Re_a for flow regimes with large δ/a, which does not extend to regimes with smaller δ/a, supports the proposition that the dominant turbulence mechanism in very thick axisymmetric turbulent boundary layers is controlled by the outer region of the layer, and that this mechanism is only dominant over the flat plate processes when δ/a is sufficiently large.

Identification of the effects of transverse curvature on the mean-velocity distribution in the inner region of the boundary layer requires the mean-velocity profiles scaled on wall variables in the form of U/U_τ as a function of $y^+ = yU_\tau/\nu$. To obtain this scaling, the wall shear stress τ_w must be evaluated so that the friction velocity U_τ can be determined.

The wall-friction coefficient $C_f = \tau_w/(\frac{1}{2}\rho U_1^2)$ has been extensively investigated for flat-plate boundary layers, but there has been some difficulty in carrying over flat-plate techniques to axisymmetric boundary layers. Willmarth et.al.(1976) demonstrated that a Preston tube with the established two-dimensional-boundary-layer calibration can be used to determine τ_w in an axisymmetric layer with values of δ/a up to about 10, provided that the tube diameter d_p is such that $d_p/a < 0.6$ and d_pU_τ/ν is small enough to

ensure that the tube is within the buffer-layer region of the boundary layer. For very small cylinders with δ/a up to 42, they determined C_f by matching the mean-velocity profile of the axisymmetric boundary layer to that of a flat-plate layer. However, Lueptow and Haritonidis (1987) show that this latter procedure tends to overestimate the friction coefficient. As an alternative, they attempted to determine C_f from the slope of the straight line representing the variation of Reynolds stress with inverse radial distance implied by the existence of a constant shear-stress moment in the wall-region of an axisymmetric turbulent boundary layer, but the method was found to suffer inaccuracies as a result of experimental data-scatter and instrumentation constraints. They place reliance on data obtained from a Preston tube small enough to be submerged within the viscous sublayer and calibrated in a flat-plate layer against a standard Preston tube. A surface-hot-wire probe, calibrated against a Preston tube, has been used by Wietrzak and Lueptow (1994) to measure both mean and fluctuating wall shear stresses in an axisymmetric layer. Wall shear stresses beneath very thick layers ($\delta/a > 100$) have been obtained by Cipolla and Keith (2003a) by measuring differences in total drag of cylinders towed in a water tank, following repeated incremental reductions in cylinder length. Nevertheless, even now, despite the wide variety of procedures that have been proposed, the most satisfactory experimental method of measuring the mean wall stress in an axisymmetric turbulent boundary layer seems to be the use of a Preston tube with dimensions constrained within the limits originally established by Willmarth et.al.(1976), in conjunction with the standard two-dimensional-flow calibration.

In the present investigation experimental measurement of the wall shear stress has not been attempted. In view of the very small diameter of the cylinder involved in this part of the investigation (0.9 mm), the use of Preston tubes or surface-hot-wire

probes was considered impracticable. Instead, following Luxton et.al.(1984), the values of the wall shear stress for the three velocity profiles under investigation here, have been obtained by interpolation of Willmarth et.al.'s (1976) results for C_f as a function of $Re_{\theta 2}$. The velocity profiles in terms of U/U_τ against y^+ are shown in Figure [4.7] together with the "law of the wall" (Coles 1955) for flat plate boundary layers and previous results by Willmarth et.al.(1976) for a range of values of δ/a. The figure clearly demonstrates the transition from flat-plate flow to flow strongly affected by curvature. At values of δ/a as high as 4, essentially flat-plate flow still persists, but as δ/a is increased the increasing transverse curvature brings about a progressive disappearance of the logarithmic region of the profile; at $\delta/a > 30$ all traces of the flat-plate logarithmic region in the velocity profile have disappeared.

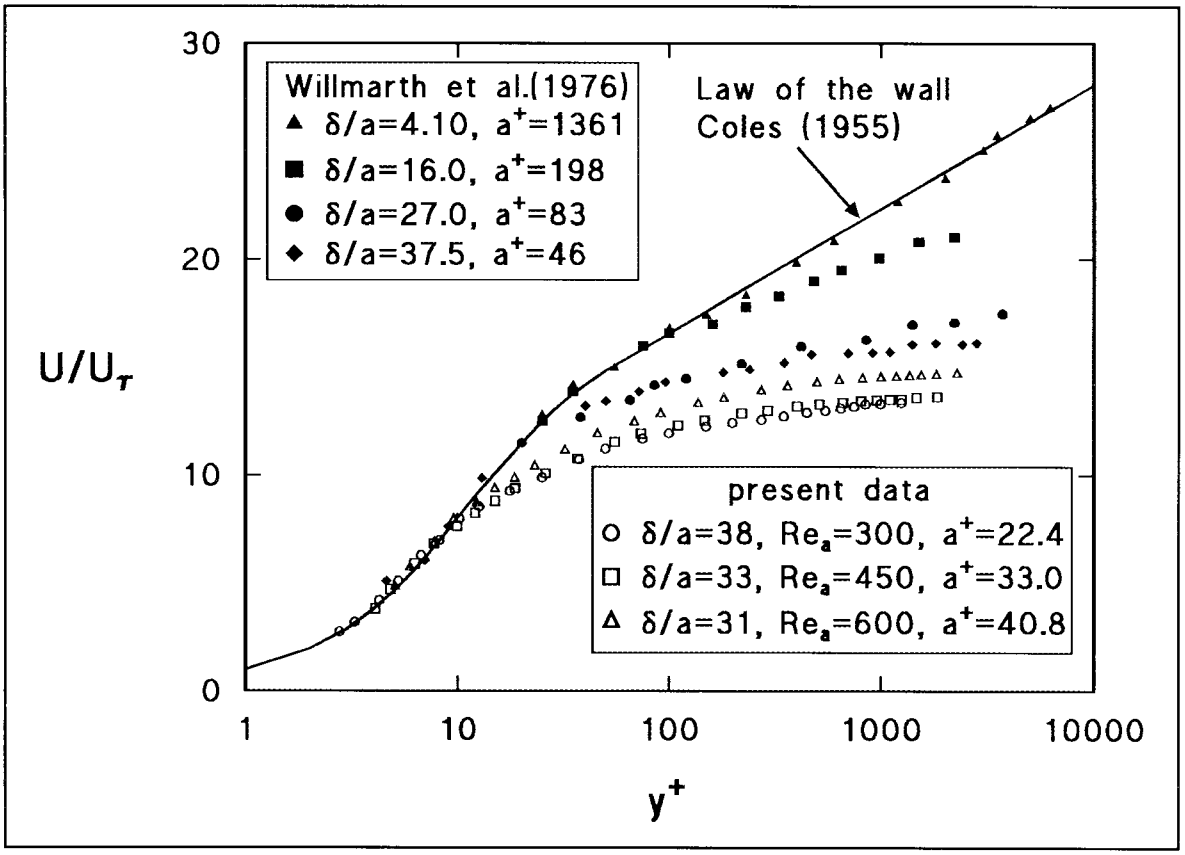

Figure 4.7 The distribution of the mean velocity scaled on wall variables, together with comparable data (Willmarth et.al.1976) at smaller values of δ/a and the "law of the wall" (Coles 1955) for flat plate boundary layers.

In the discussion of their results, Willmarth et.al.(1976) applied an argument by Rao (1967) that the equations for the mean flow very near the surface will be dominated by the viscous terms, and that, in the absence of a pressure gradient, the shearing force $2\pi r\mu\partial U/\partial r$ per unit length acting on a cylinder of fluid must be constant. Hence the mean velocity must be proportional to the logarithm of r, and that with U = 0 at r = a:

$$U/U_\tau = a^+\ln(1+y^+/a^+) \quad . \qquad [4.13]$$

The inner region of the boundary layer, as shown in Figure [4.7], is shown to a larger scale in Figure [4.8], together with Equation [4.13] for $a^+ = 33$ (there is very little difference in the curve for Equation [4.13] for the different a^+ used here). The present

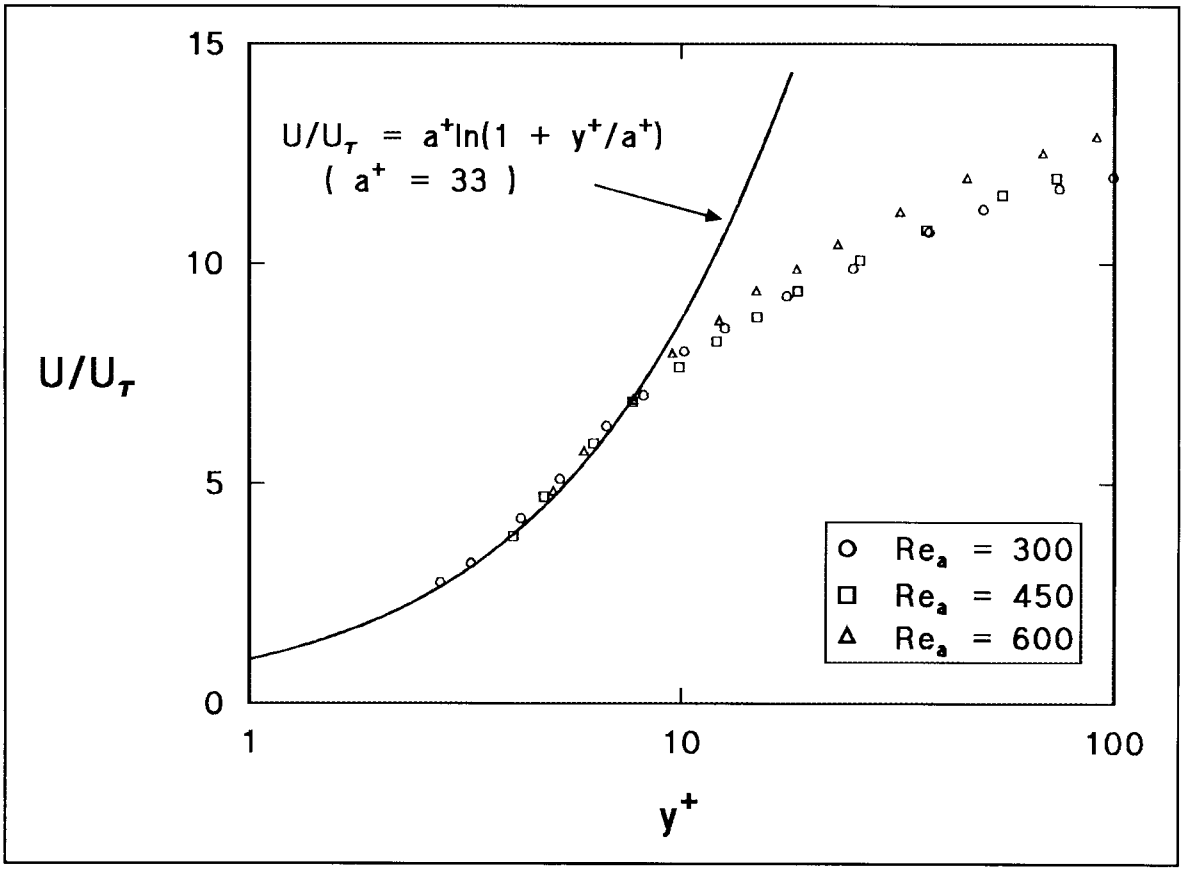

Figure 4.8 The mean velocity distribution scaled on wall variables for small y^+, together with a theoretical expression for inner layer velocities (Rao 1967).

data behave as predicted in the inner region, suggesting a broader extent of similarity of the inner regions of axisymmetric boundary layers for all δ/a.

The mean properties of the thick axisymmetric turbulent boundary layers formed on a long slender cylinder in axial flow which have been investigated in the present work are summarised in Table [4.1].

U_1 m/s	Re_a -	δ mm	δ/a -	δ^* mm	δ_1^* mm	δ_2^* mm	θ mm	θ_1 mm	θ_2 mm	U_τ m/s	a^+ -	x/a -
10.35	300	16.9	38	1.18	15.3	3.29	0.98	14.5	3.19	0.77	22.4	6000
15.19	450	14.9	33	0.79	7.86	2.25	0.64	7.50	2.19	1.11	33.0	6000
19.96	600	13.8	31	0.71	7.07	2.11	0.59	6.76	2.06	1.36	40.8	6000

Table 4.1 Mean properties of the axisymmetric turbulent boundary layer at Reynolds number Re_a = 300, 450 and 600 for a cylinder with radius a = 0.45 mm at a streamwise location x = 2700 mm (x/a = 6000). The boundary layer thickness δ is estimated as δ = y at U/U_1 = 0.99. The friction velocity U_τ and the nondimensional radius a^+ are determined from a wall shear stress τ_w estimated using the procedure adopted by Luxton et.al.(1984).

4.1.2 Fluctuating properties of the axisymmetric boundary layer

Measurements of the longitudinal velocity fluctuation u have been made by sampling the calibrated output from a hotwire probe at 20 kHz, after filtering the analogue signal with a low pass filter set at 10 kHz. Sample sizes of 32,000 data points were recorded for each measurement position, providing a record of the longitudinal velocity fluctuation of 1.6 seconds duration.

All of the measurements were conducted at the same axial location, x/a = 6,000, where the mean velocity profiles were also determined. Velocity samples were recorded at a series of radial locations throughout the boundary layer from y = 0.1 mm to y = 25 mm, at each of the Reynolds numbers Re_a of 300, 450 and 600.

The distribution throughout the boundary layer of u'/U_1, the relative magnitude of the rms longitudinal velocity fluctuations, is shown as a function of y/θ for different Reynolds numbers Re_a in Figure [4.9(a)] and as a function of y/δ in Figure [4.9(b)]. In the latter, the distribution of u'/U_1 in a two-dimensional flat-plate boundary layer, as measured by Klebanoff (1955), is also shown. The principal features of the distribution of turbulence intensity are the very high values of u'/U_1 found close to the cylinder surface (some 50% greater than in the flat plate layer) and, as y/θ and y/δ increase, the rapid decrease in intensity values that, over most of the layer, are considerably lower than those for the flat-plate. Luxton et.al.(1984) have proposed that similar distributions of turbulence intensity found in their investigations may result from large outer layer structures "peeling off" the inner-layer fluid as they sweep transversely across the

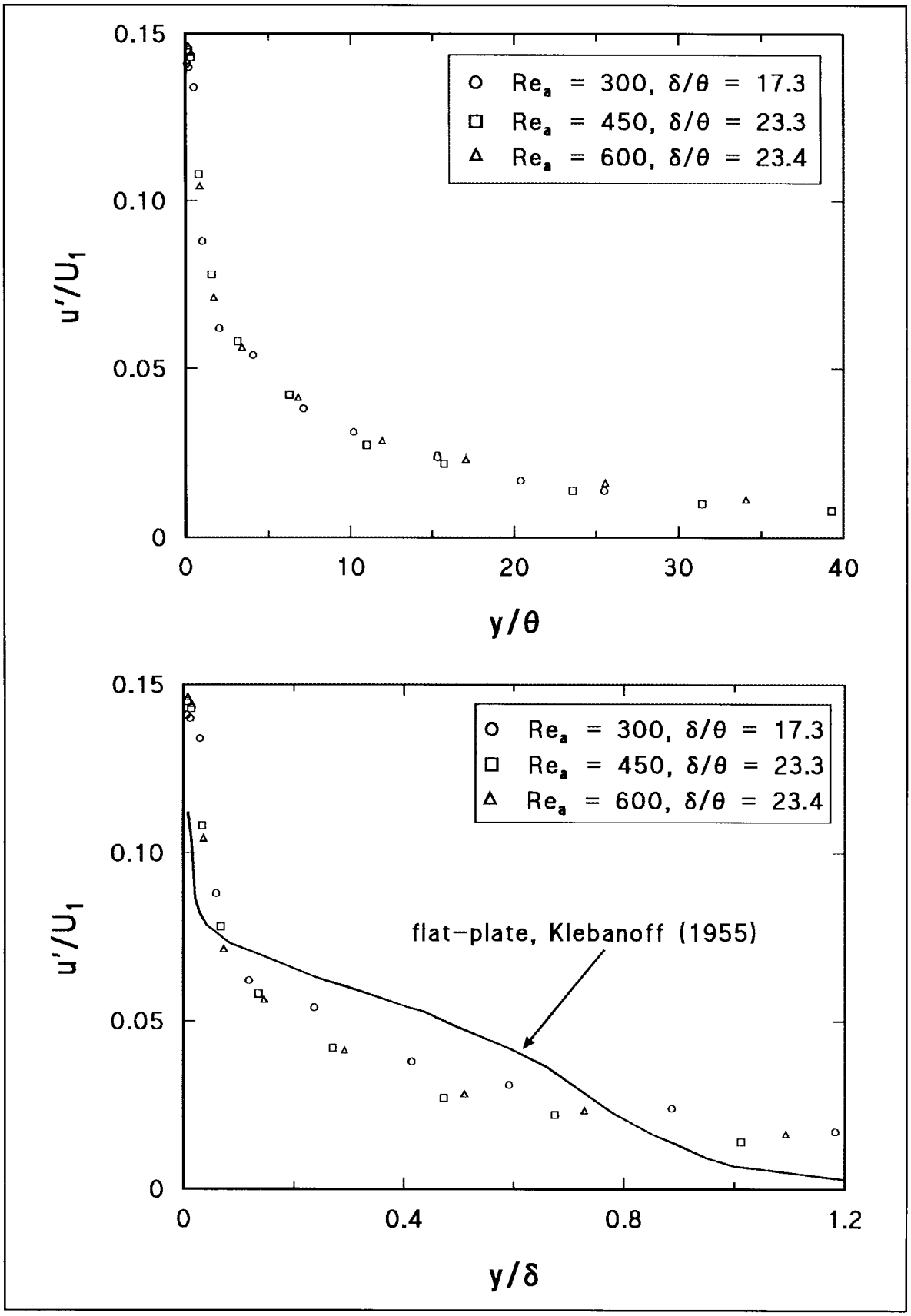

Figure 4.9 The distribution of rms longitudinal velocity fluctuation: (a) with y/θ (upper) and (b) with y/δ together with flat plate data (Klebanoff 1955) (lower).

cylinder, a process not possible in a flat-plate boundary layer where the movement of such structures is blocked by the presence of the wall.

The intermittent removal of inner layer fluid which has a characteristic velocity of order U_τ, and its consequent replacement with higher-velocity fluid from the outer layer, which has a characteristic velocity of order U_1, would produce large random variations in the longitudinal velocity close to the surface and a consequent increase in the rms value of the local longitudinal velocity fluctuations. Similarity across the range of Reynolds numbers observed for the mean velocity distribution is also shown by the distribution of turbulence intensity (Figure [4.9]) scaled on outer-flow variables.

Some further insight into the nature of the turbulence mechanisms in the axisymmetric boundary layer can be obtained from the skewness factor

$$S = \frac{\overline{u^3}}{\left(\overline{u^2}\right)^{\frac{3}{2}}} \qquad [4.14]$$

and the flatness factor

$$F = \frac{\overline{u^4}}{\left(\overline{u^2}\right)^2} \qquad [4.15]$$

of the longitudinal velocity fluctuations. The distribution of S and F with y/θ and y/δ for different Re_a are shown in Figures [4.10] and [4.11] respectively. In Figures [4.10(b)] and [4.11(b)] Klebanoff's (1955) experimental values for a flat-plate boundary layer are also shown. Over the range of Reynolds numbers in the axisymmetric flow, the skewness shows similarity with outer-flow-variable scaling for y/δ up to about 0.2 and similarity of trends at larger y/δ, while for the flatness the similarity extends as far as $y/\delta = 1$. As for the distribution of turbulence intensity, distinct differences appear

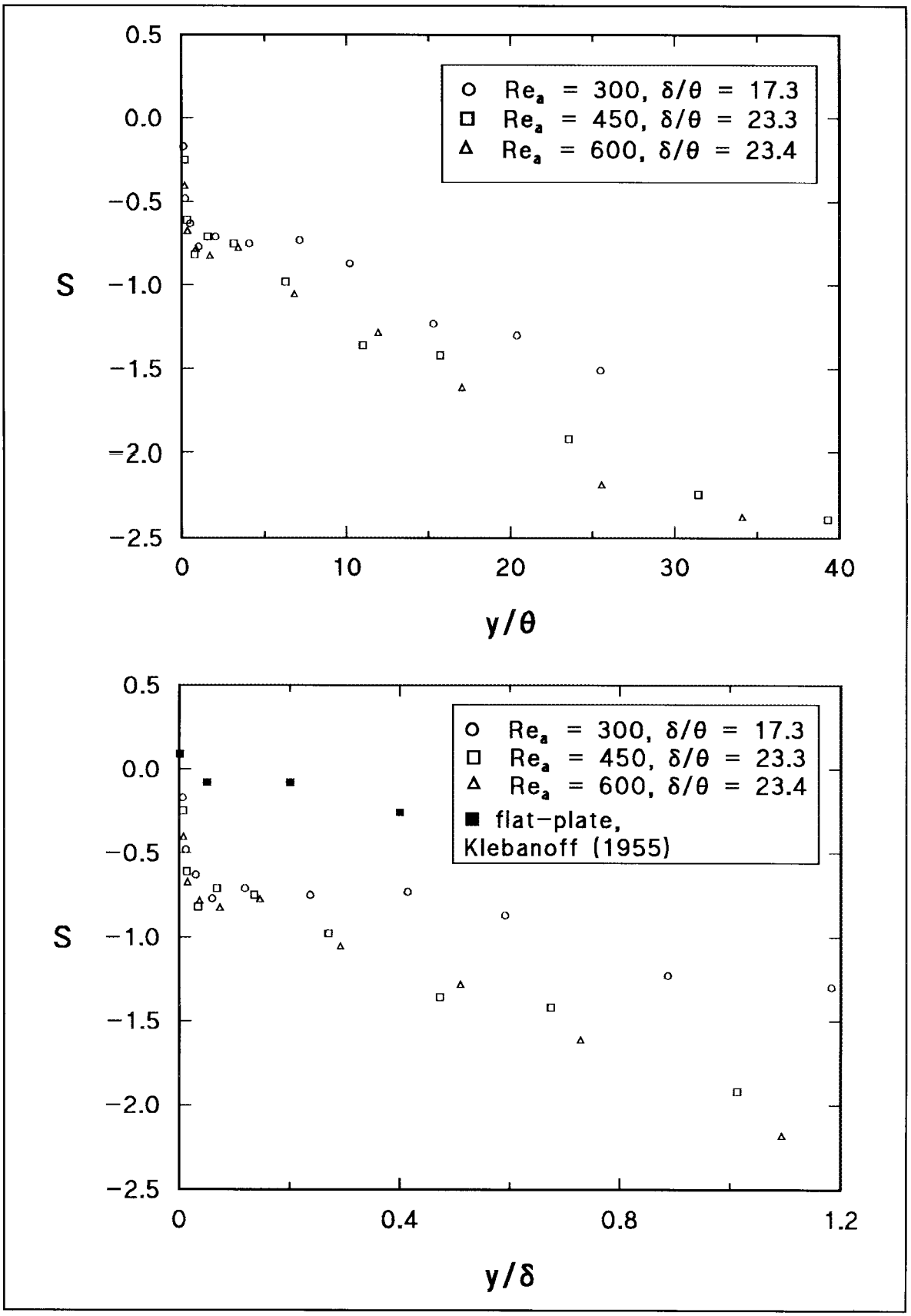

Figure 4.10 The distribution of the skewness factor S: (a) with y/θ (upper), and (b) with y/δ together with flat plate data (Klebanoff 1955) (lower).

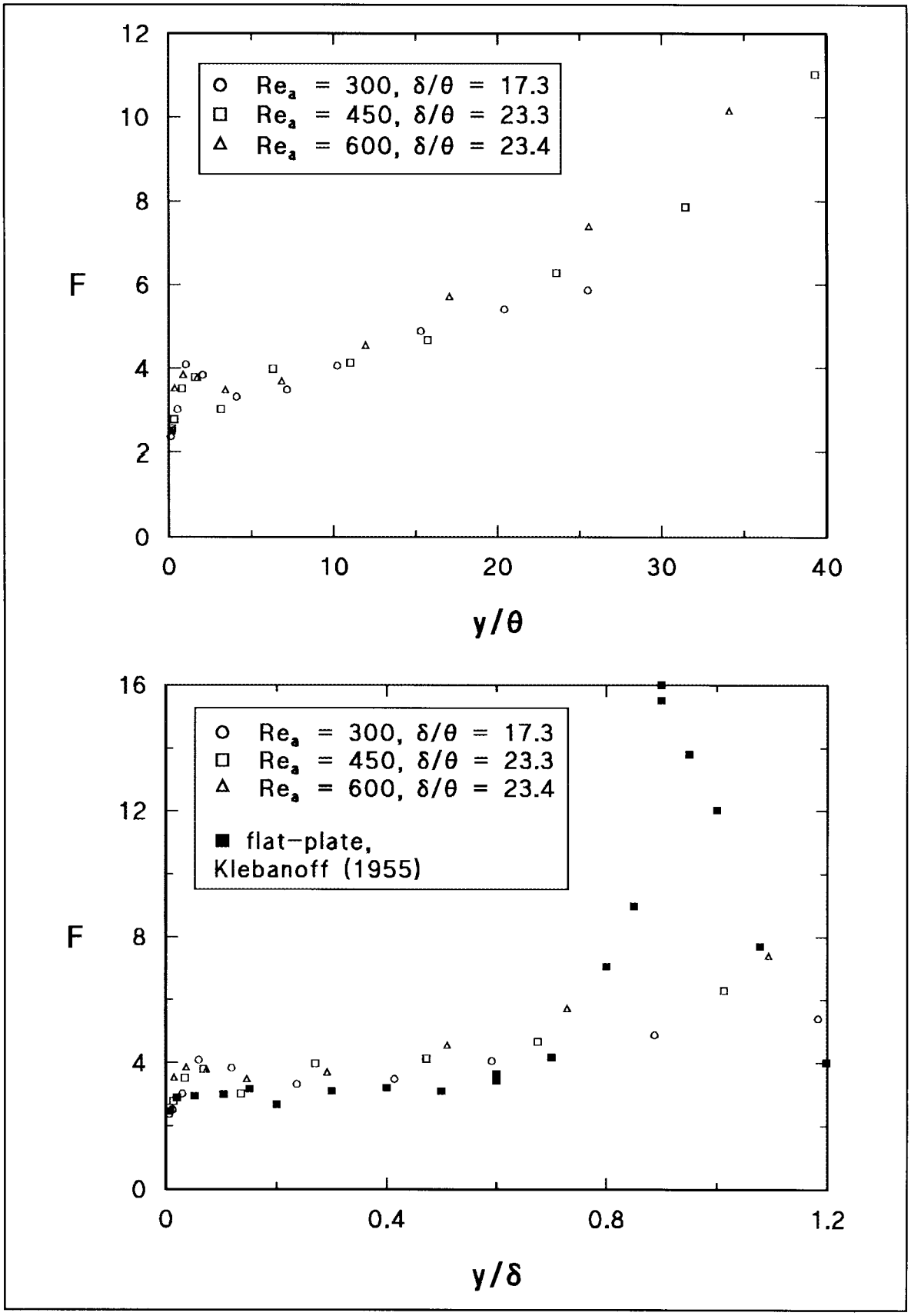

Figure 4.11 The distribution of the flatness factor F: (a) with y/θ (upper), and (b) with y/δ together with flat plate data (Klebanoff 1955) (lower).

between the inner and outer regions, supporting the notion of the existence of two different length scales and their associated turbulence mechanisms: a small inner scale possibly associated with mechanisms similar to those occurring in a flat-plate layer, and a larger scale characteristic of the thick boundary layer resulting from the effects of transverse curvature.

A skewness factor that is negative throughout the boundary layer, and generally of a magnitude very much greater than that of a flat-plate boundary layer (Figure[4.10(b)]), lends support to the suggestion that inner-layer low-velocity fluid is being stripped away from the cylinder surface and carried outwards through the boundary layer, producing large local negative velocity fluctuations in the outer layer. The variation of flatness (kurtosis) factor with y/δ (Figure [4.11(b)]) is similar to that in the flat-plate layer for $0 \leq y/\delta \leq 0.7$, but the flatness is significantly higher than the flat-plate value, indicating a greater departure of the longitudinal velocity fluctuations from a normal distribution. For $0.7 \leq y/\delta \leq 1.1$, F increases but does not reach such large values as for the flat-plate layer (similarly large values are reached only at radial distances much larger than the boundary layer thickness (Figure [4.11(a)])). This implies lower intermittency in the outer part of the axisymmetric layer, which would seem to be consistent with the postulated process of inner-layer-stripping. Probability-density functions of the longitudinal velocity fluctuations, shown in Figure [4.12] for $Re_a = 450$ at different radial positions y/θ, clearly indicate the increased negative skewness, as compared with flat-plate flow, at each location in the boundary layer.

Similarity over the range of Reynolds number examined here of the probability-density function of the longitudinal velocity fluctuations is shown in Figure [4.13] for the inner region at $y/\theta \approx 0.18$, and in Figure [4.14] for the outer region at $y/\theta \approx 6.8$. Comparison of these probability distributions for the inner and outer regions of the boundary layer indicates that the inner-region velocity varies over a wider range with a slight negative skewness, whereas the outer-region velocity is concentrated over a smaller range of variation with a more pronounced negative skewness. These results are consistent with an inner-flow with the character of a continuously-regenerating boundary layer, and an outer flow characterised by a more uniform velocity with a low level of turbulence with frequent spots of very low velocity due to the passage of inner layer fluid which has been removed from near the cylinder surface.

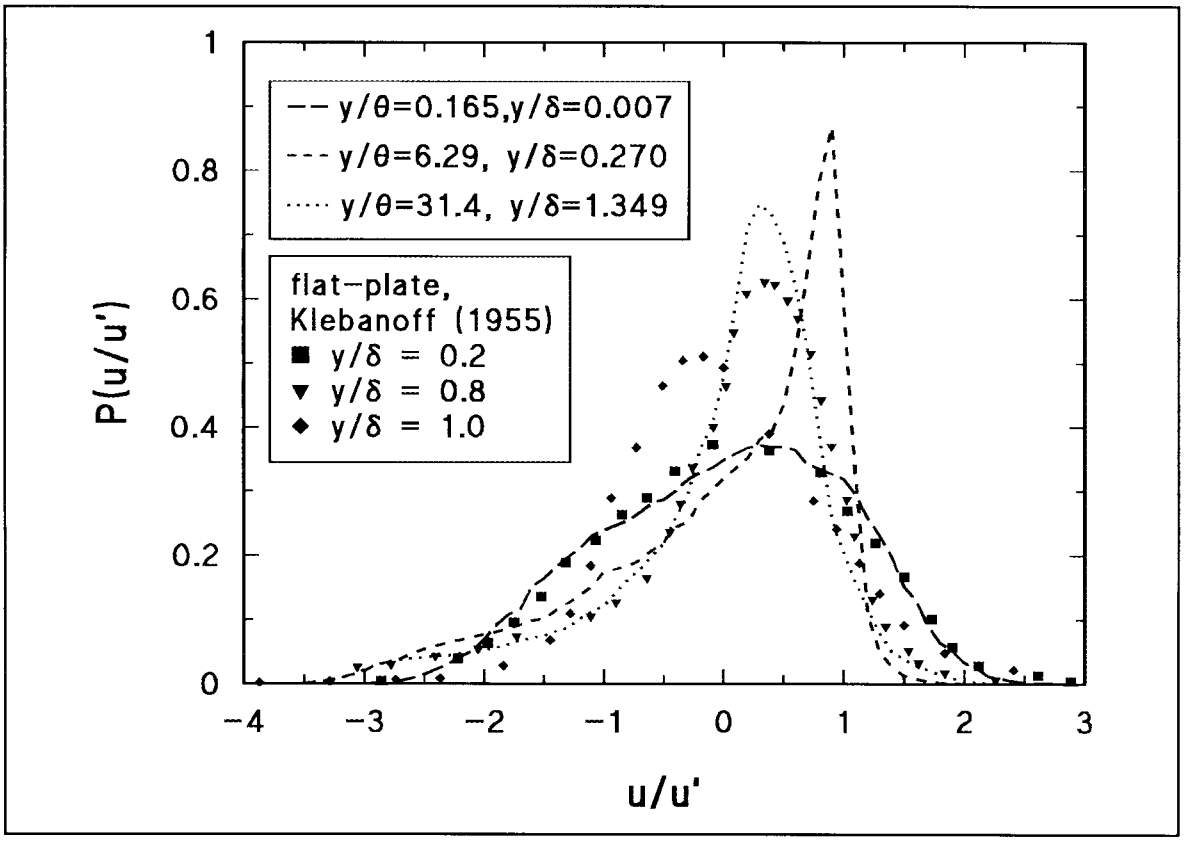

Figure 4.12 The distribution of the probability density function P(u/u') at different y/θ for $Re_a = 450$, together with flat plate data (Klebanoff 1955).

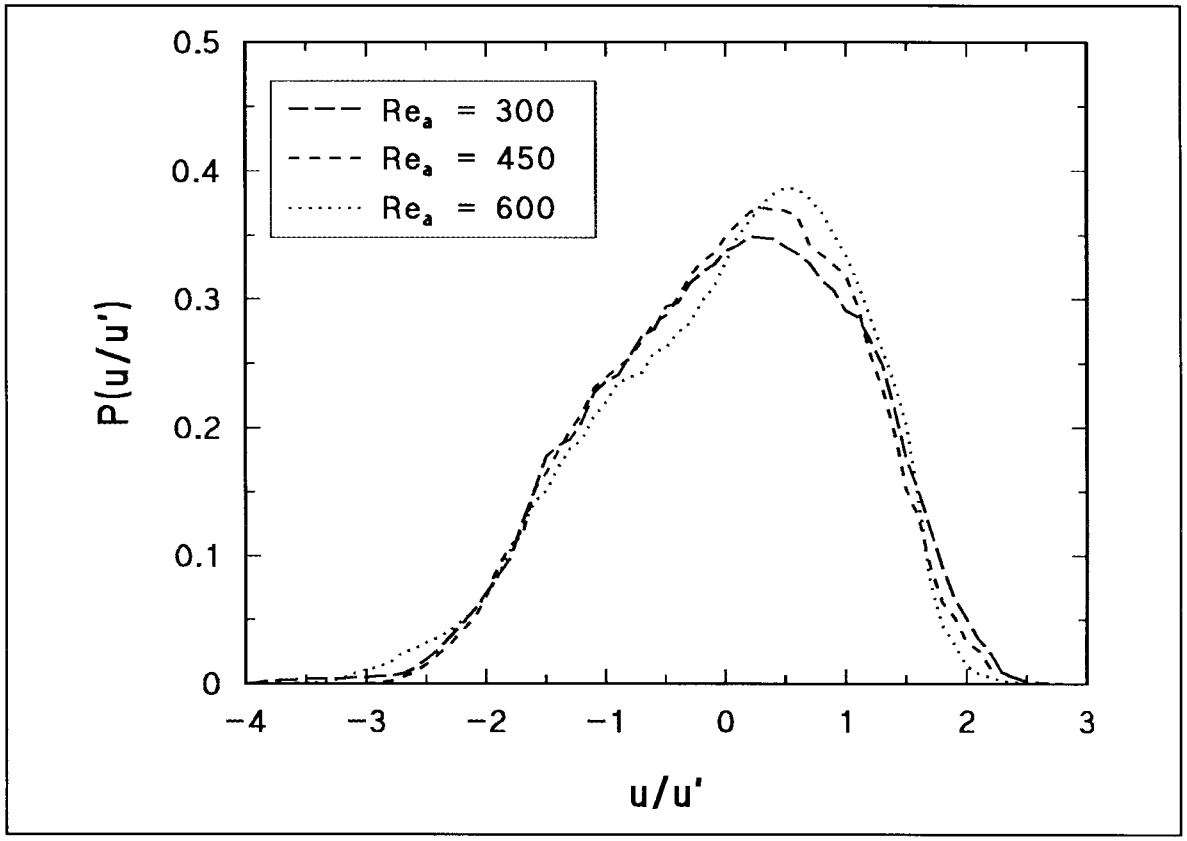

Figure 4.13 The distribution of the probability density function P(u/u′) at different Re_a for $y/\theta \approx 0.18$ (Re_a 300, $y/\theta = 0.21$; Re_a 450, $y/\theta = 0.17$; Re_a 600, $y/\theta = 0.18$).

The statistical examination of the longitudinal velocity fluctuations indicates that the apparent differences between the flow mechanisms within the thick turbulent boundary layer generated on a long slender cylinder in axial flow and those within a turbulent flat plate boundary layer are associated with the existence of large negative spikes in the fluctuating velocity record. The proposition that such local 'spots' of low velocity are the result of inner-layer low-speed fluid being stripped away from the cylinder surface by large scale turbulent structures flowing across the cylinder, without the usual deterrence of the wall, will be examined in greater detail in chapter seven.

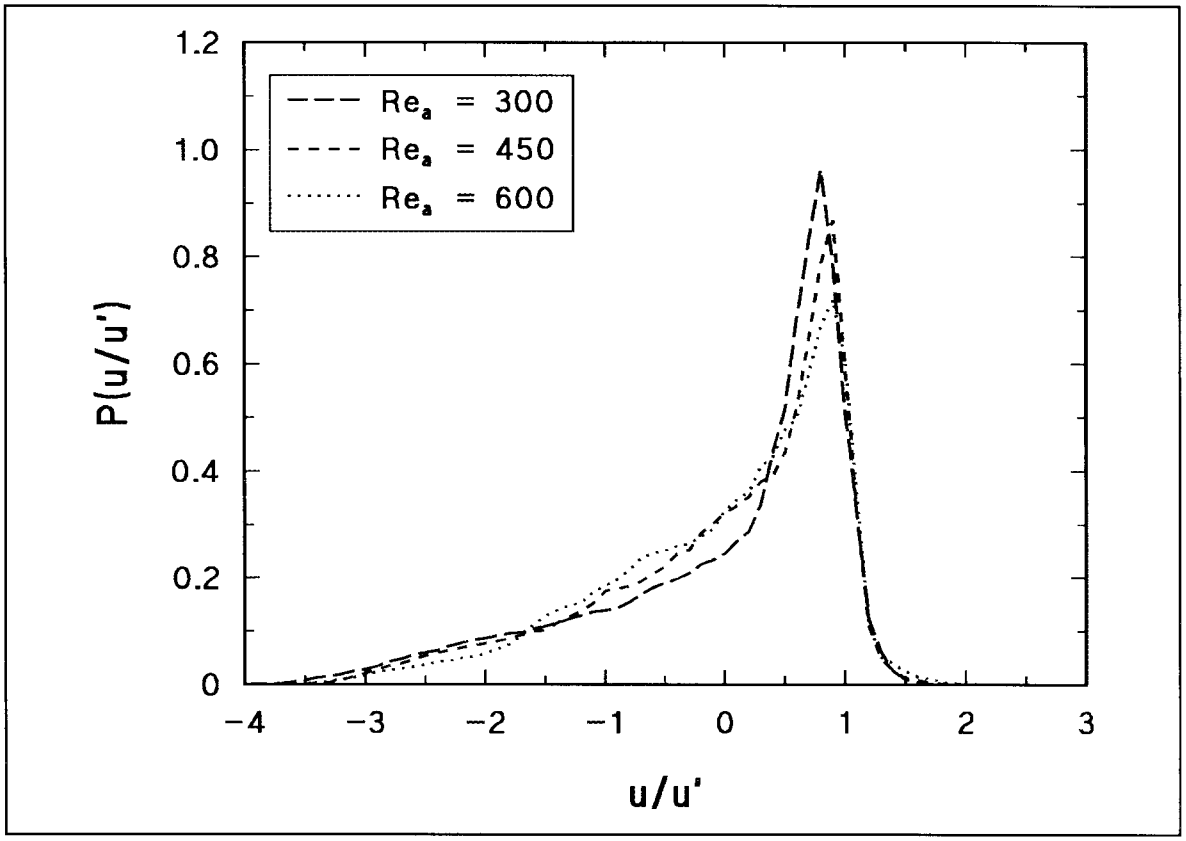

Figure 4.14 The distribution of the probability density function P(u/u') at different Re_a for $y/\theta \approx 6.8$ (Re_a 300, $y/\theta = 7.1$; Re_a 450, $y/\theta = 6.3$; Re_a 600, $y/\theta = 6.8$).

4.2 The Long Slender Cylinder in Near-axial Flow

Numerous previous researchers in reporting investigations of axisymmetric boundary layers have noted the extreme precision in geometrical alignment of the cylinder required to produce axisymmetric boundary layers. This degree of experimental difficulty implies that the boundary layer symmetry is very sensitive to the cylinder yaw angle β, defined such that $\beta = 0°$ corresponds to axial flow along the cylinder, and $\beta = 90°$ corresponds to flow across the cylinder.

Some guidance for the present investigation was provided by an investigation of the effect of cross flow on the boundary layer on a circular cylinder by Willmarth et.al.(1977) for Re_a 4900, $\beta = 1.06°$ and Re_a 39,000 $\beta = 2.36°$,6.62°, where the asymmetry was so pronounced that for yaw angles above 1° the windward boundary layer thickness was found to be too thin to be measured, and at $\beta = 2.36°$ the leeward boundary layer was found to exhibit a wake like behaviour.

The present investigation at much smaller Reynolds numbers has identified regular vortex shedding at angles as small as $\beta = 2°$, and wake-like irregular shedding of the shear layers at smaller angles in the order of $\beta = 1°$. For the range of Reynolds numbers in the current investigation the region of yawed asymmetric turbulent boundary layers is restricted to $\beta < 1°$. At larger yaw angles the extent of flow separation from the leeward side of the cylinder produces a flow regime with more in common with the behaviour of cylinders normal to the flow than with cylinders axially aligned with the flow.

4.2.1 Mean properties of the yawed-cylinder boundary layer

The mean velocity throughout the yawed-cylinder boundary layer has been measured in the same manner as for the axisymmetric boundary layer, with the exception that measurements very close to the cylinder surface were restricted to a minimum value of y = 0.08 mm.

The measurement of the radial position of the hot wire probe could not be made with the same accuracy as obtained in the axial case due to the absence of symmetry in the flow, and thus the initial location of each probe traverse was measured to ± 0.05 mm using the optical technique. As subsequent measurements were made with the accuracy of the surface gauge traverse mechanism of ± 0.01 mm, the maximum error in the measurement of the probe location appears as a fixed offset value $\leq$ 0.05 mm, which implies that only the inner measurements at small y may be affected by significant errors.

With the cylinder yawed in the vertical plane, and the yaw angle measured from the previously determined axial position, measurements were made of the mean velocity distribution on both the windward and leeward sides of the inclined cylinder for yaw angles of 0.25° and 0.50°. The measured velocity profiles of the yawed cylinders are shown together with the axisymmetric velocity profile for the same Reynolds number in Figures [4.15] for Re_a = 300, [4.16] for Re_a = 450 and [4.17] for Re_a = 600 as U/U_1 against the radial coordinate y (perpendicular to the cylinder axis in all cases). In all cases the boundary layer becomes thinner, and the profile shape fuller, on the windward side with increasing β, with the opposite effect occurring on the leeward side.

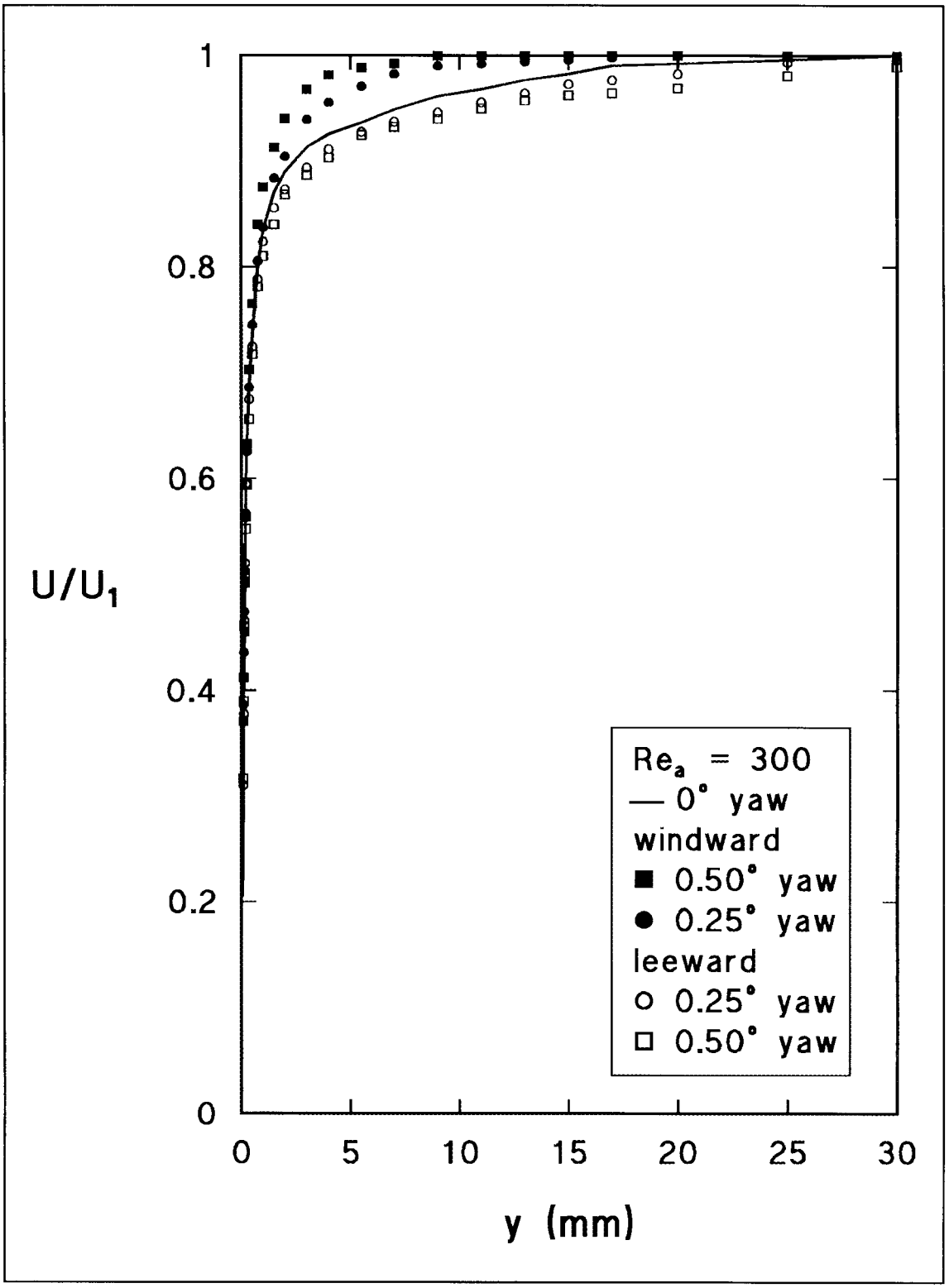

Figure 4.15 Distribution of mean velocity in the boundary layer at different angles of cylinder yaw for Re_a = 300.

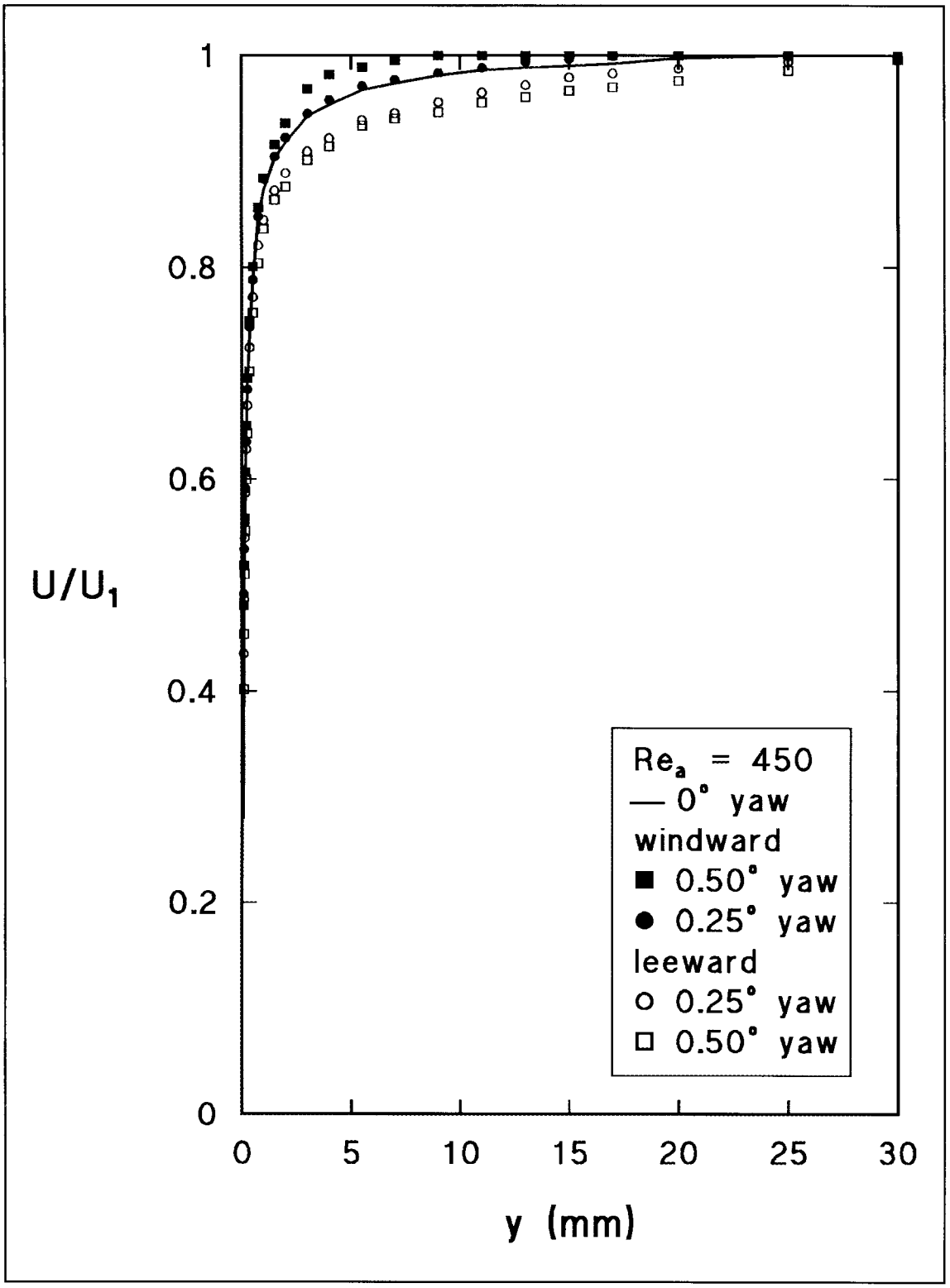

Figure 4.16 Distribution of mean velocity in the boundary layer for different angles of cylinder yaw for Re_a = 450.

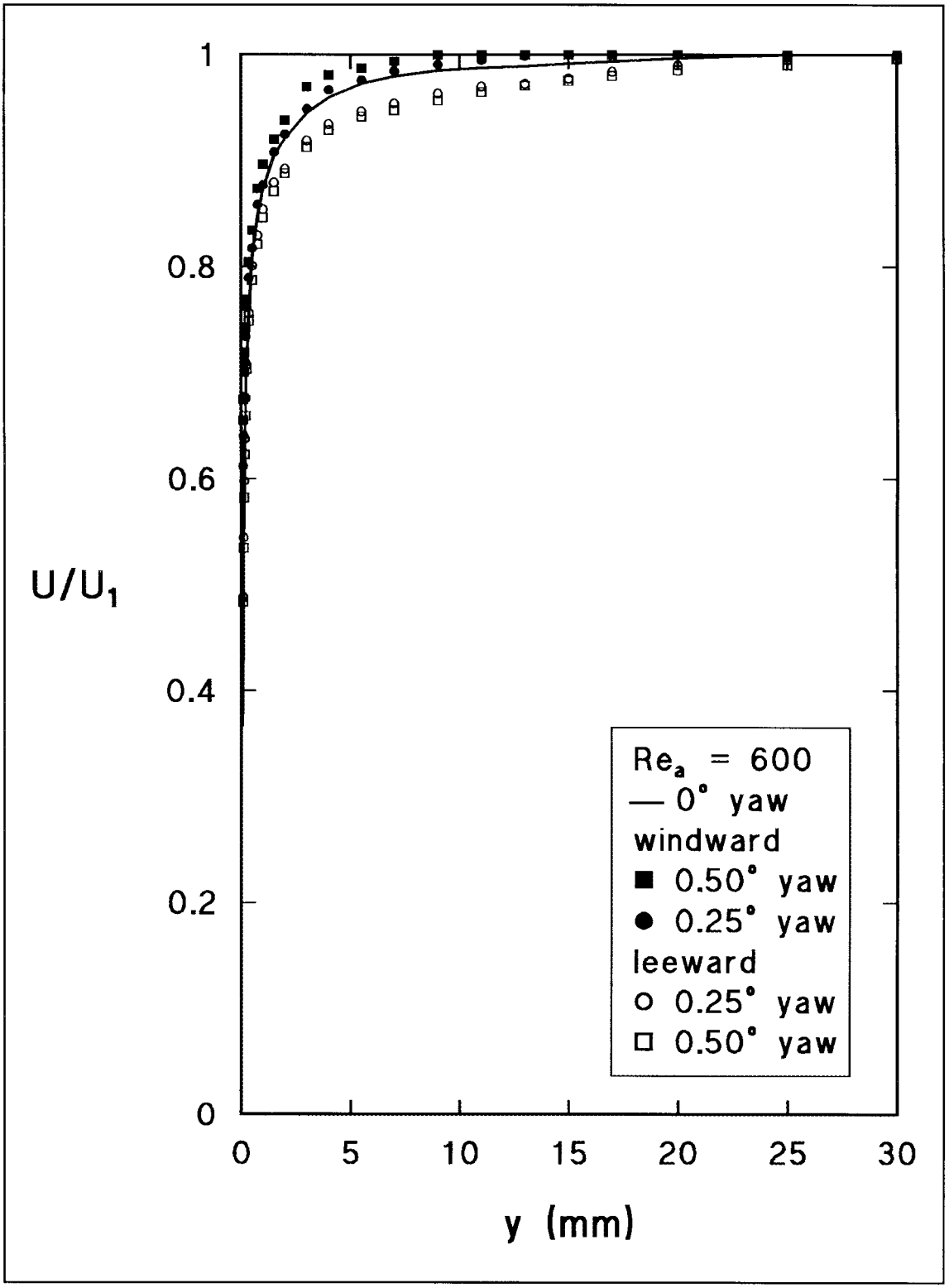

Figure 4.17 Distribution of mean velocity in the boundary layer at different angles of cylinder yaw for Re_a = 600.

4.2.2 Asymmetry of the boundary layer due to cylinder yaw

Approximate contours of constant mean velocity in a plane perpendicular to the cylinder axis (the yz plane as shown in Figure [4.18]) are plotted in Figures [4.19] to [4.24] for each combination of yaw angle and Reynolds number. It has been assumed that the contours are elliptical. For a given value of U/U_1, the windward and leeward extremities of the major axis ($y = -y_L$ and $y = y_L$) have been obtained from the mean-velocity profiles of Figures [4.15] to [4.17]. (Note that in Figures [4.15] to [4.17] y is used as a radial coordinate, the distance from the cylinder surface. Here y is a cartesian coordinate with its origin at the cylinder axis.) To determine the minor axis of the ellipse, the radial distance to the contour from the cylinder axis r_c has been assumed to vary linearly between its windward and leeward values with y_c the y-coordinate of the contour. This assumption appears to be consistent with the more comprehensive measurements around constant-velocity contours made by Willmarth et al. (1977) for a yaw angle of $\beta = 1.06°$.

As the greater part of the velocity variation across each boundary layer occurs in the inner layer, this region is drawn to a larger scale (x8) for each configuration. Constant velocity contours for $U/U_1 = 0.66$, 0.82, 0.87, 0.90, 0.955, 0.98 and 0.995 are shown in Figures [4.19] to [4.24] for $Re_a = 300$, 450 and 600, and with $\beta = 0.25°$ and 0.50°. In each figure the contours (circles) of constant mean velocity for the axisymmetric boundary layer at the same Reynolds number are also shown for the same values of U/U_1.

Comparison of the different velocity contour plots indicates a dramatic increase in asymmetry with increasing yaw angle, and a very significant asymmetry at even the small yaw angle of $\beta = 0.25°$. For each configuration of Re_a and β, the degree of asymmetry increases with radial position from the cylinder surface. However, the innermost contour drawn here is not greatly different from the axisymmetric contour. This suggests that the innermost layers of the fluid behave in a similar manner to those of the axisymmetric boundary layer. No consistent effect of Reynolds number is shown for the limited range of Re_a covered by this investigation.

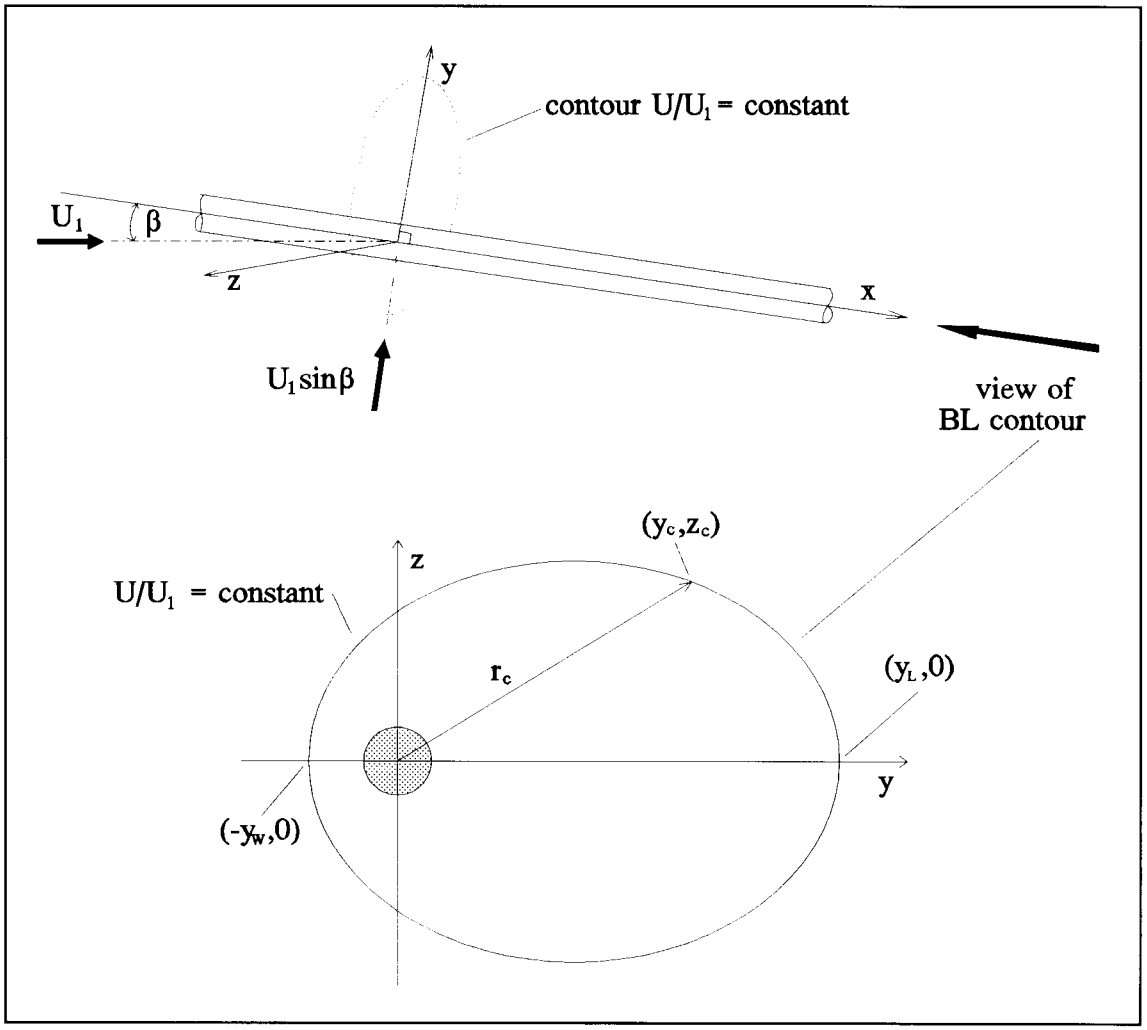

Figure 4.18 Determination of the minor-axis length of elliptical constant-velocity contours. (For the elliptic contours, the semi-minor-axis of the ellipse is given by $\sqrt{y_w y_L}$.)

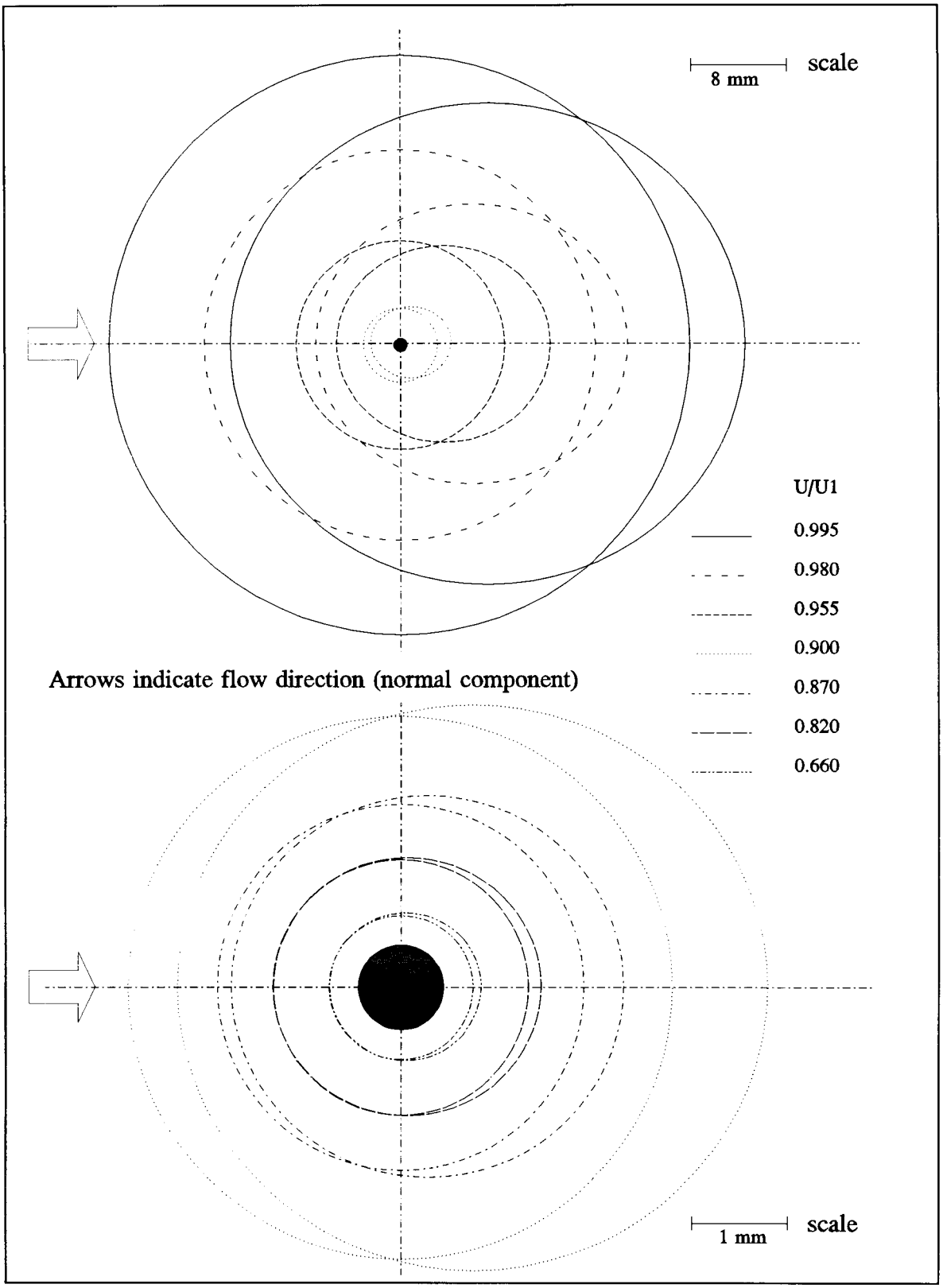

Figure 4.19 Constant velocity contours in the boundary layer for Re_a = 300, cylinder yaw angle β = 0.25°. The axisymmetric boundary layer at the same Reynolds number is shown for comparison. Lower diagram is the inner region to a larger scale.

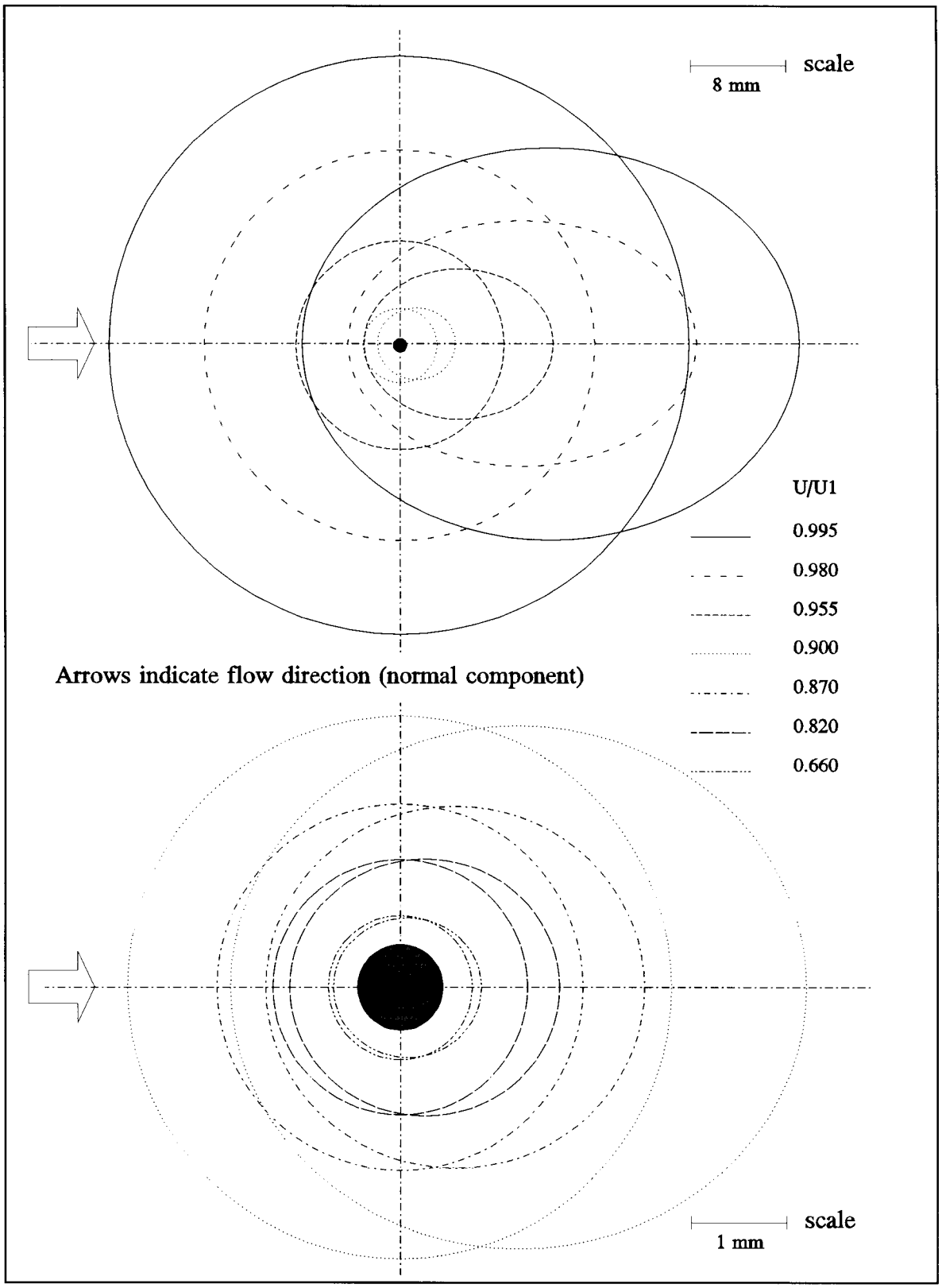

Figure 4.20 Constant velocity contours in the boundary layer for Re_a = 300, cylinder yaw angle β = 0.50°. The axisymmetric boundary layer at the same Reynolds number is shown for comparison. Lower diagram is the inner region to a larger scale.

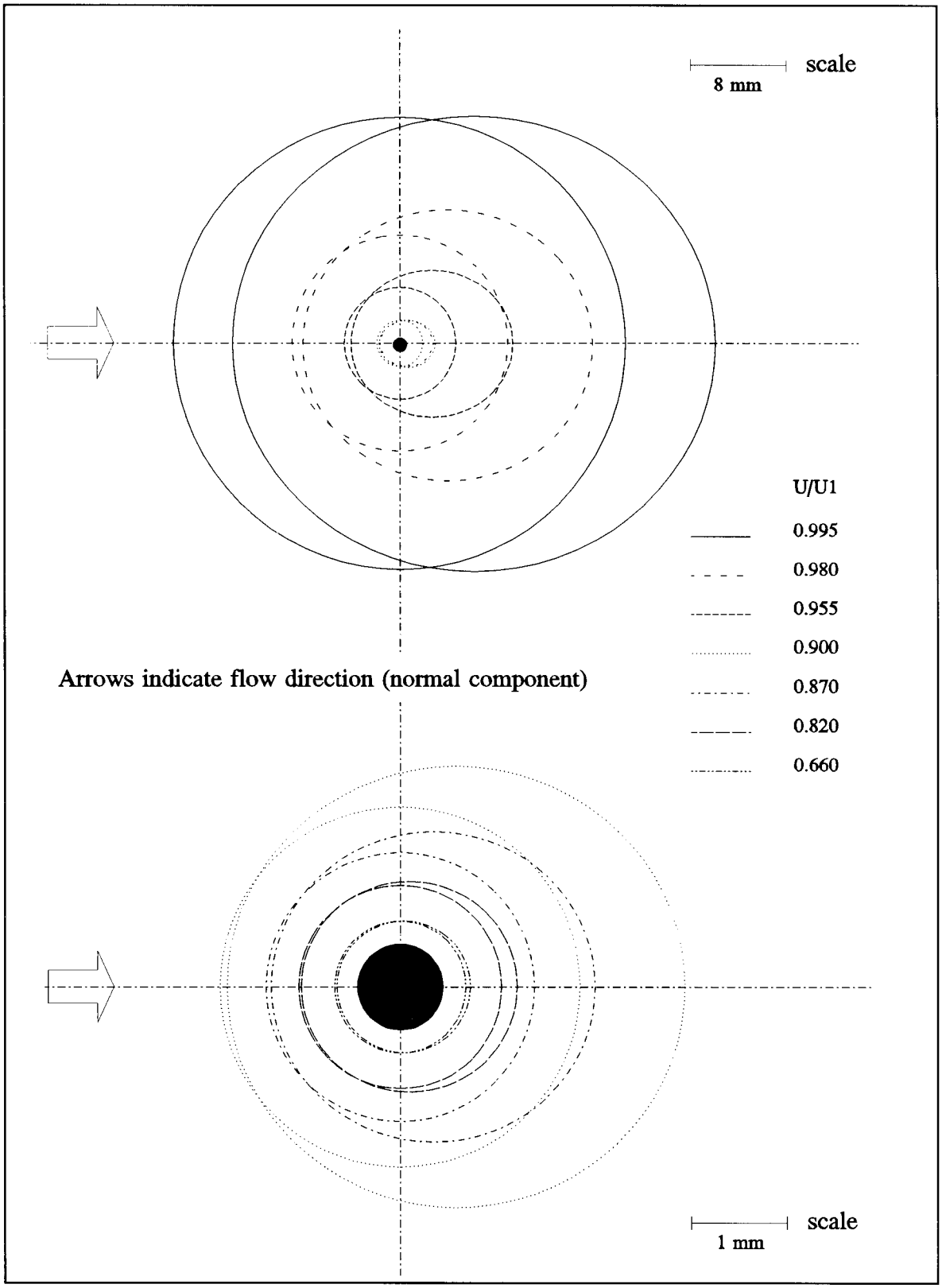

Figure 4.21 Constant velocity contours in the boundary layer for Re_a = 450, cylinder yaw angle β = 0.25°. The axisymmetric boundary layer at the same Reynolds number is shown for comparison. Lower diagram is the inner region to a larger scale.

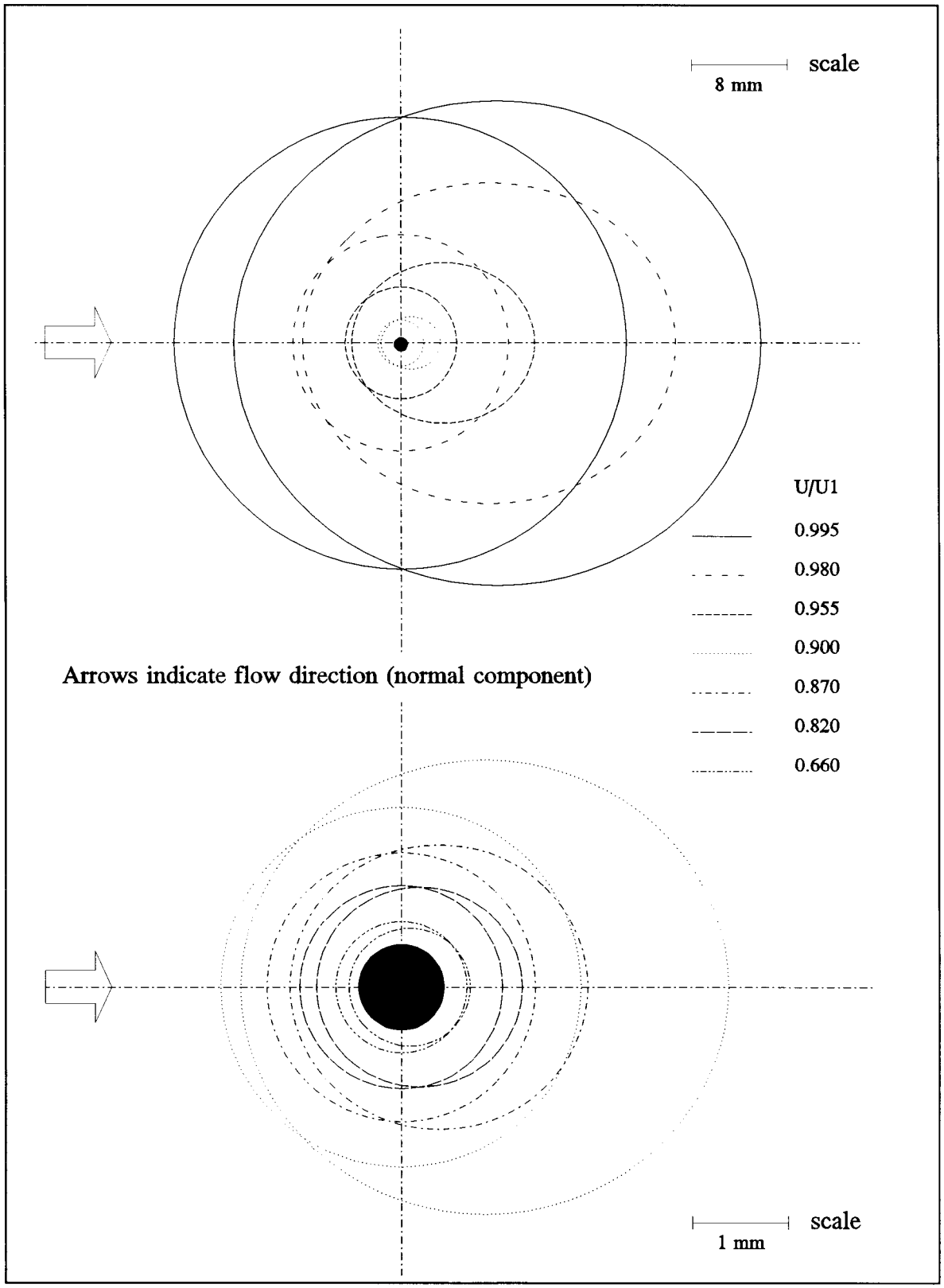

Figure 4.22 Constant velocity contours in the boundary layer for Re_a = 450, cylinder yaw angle β = 0.50°. The axisymmetric boundary layer at the same Reynolds number is shown for comparison. Lower diagram is the inner region to a larger scale.

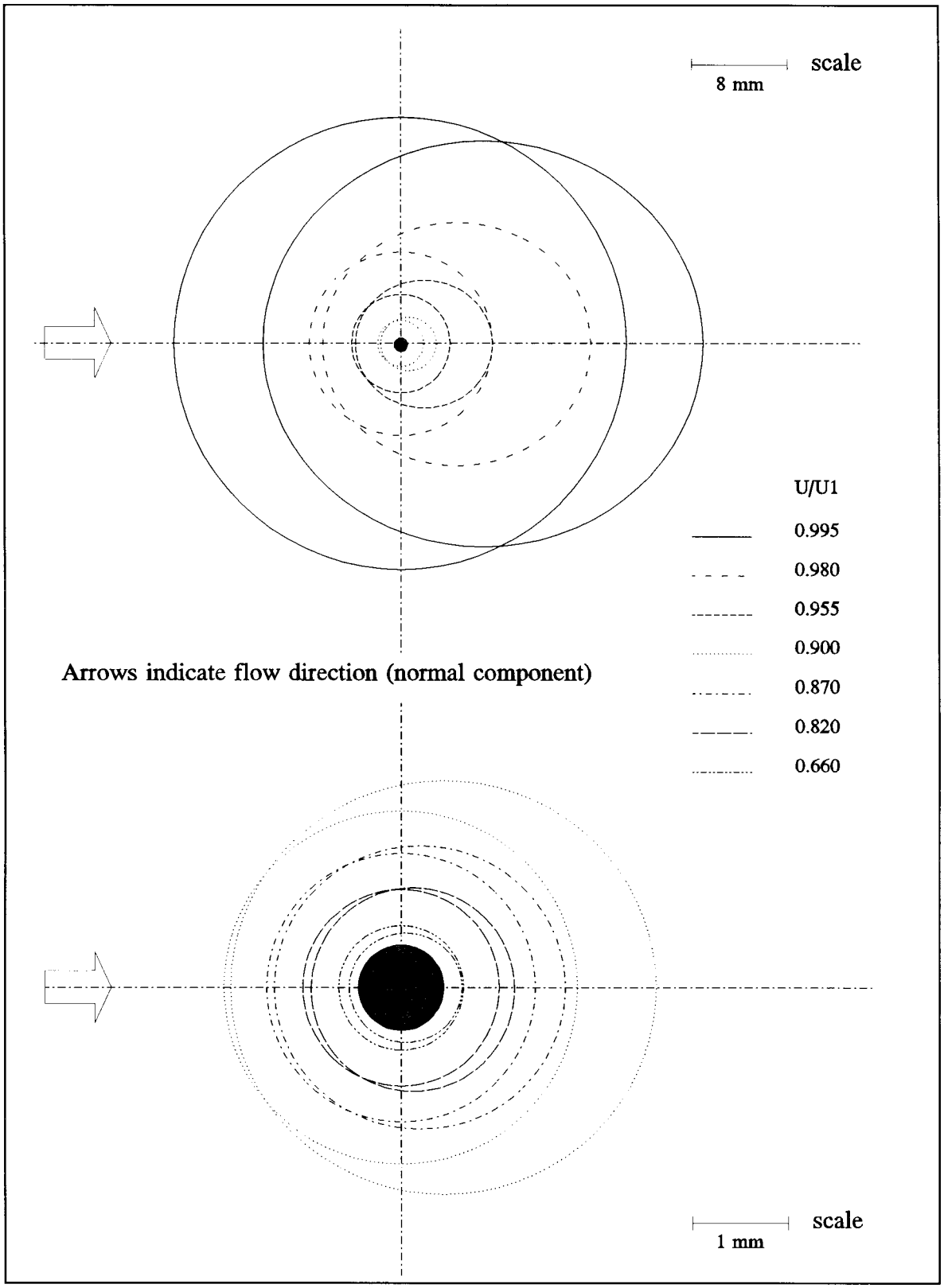

Figure 4.23 Constant velocity contours in the boundary layer for Re_a = 600, cylinder yaw angle β = 0.25°. The axisymmetric boundary layer at the same Reynolds number is shown for comparison. Lower diagram is the inner region to a larger scale.

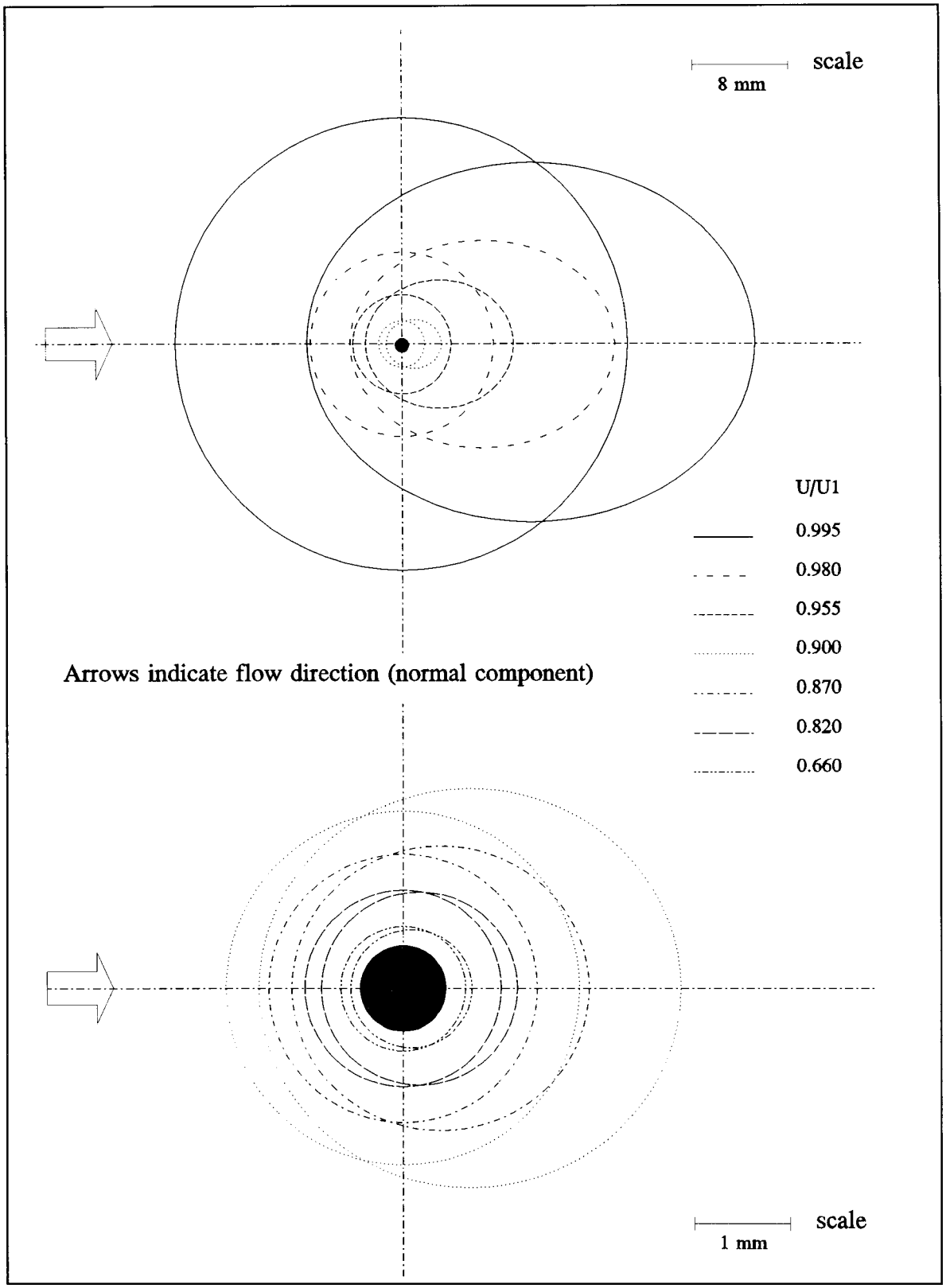

Figure 4.24 Constant velocity contours in the boundary layer for Re_a = 600, cylinder yaw angle β = 0.50°. The axisymmetric boundary layer at the same Reynolds number is shown for comparison. Lower diagram is the inner region to a larger scale.

The boundary layer properties for yaw angles greater than 0.5° were not investigated, as regular periodic fluctuations in the velocity on the lee side of the cylinder were observed for yaw angles $> 0.5°$. These oscillations indicate boundary-layer separation from the cylinder in the form of a vortex wake; this type of flow is considered further in chapters five and six.

The flow regimes investigated here are thus defined as an axisymmetric boundary layer for a cylinder in axial flow, an asymmetric boundary layer for a cylinder yawed to the flow with $0° \leq \beta° \leq 0.5°$, and a separating boundary layer, resulting in a wake flow with the possibility of regular vortex shedding for $\beta > 0.5°$.

The change from an axisymmetric boundary layer to a separating flow, similar to that over a cylinder normal to the flow, within such a small variation in yaw angle indicates the need for extreme accuracy in aligning the test cylinder to achieve axial flow. The results presented here, and the further investigations of the axisymmetric boundary layer turbulence mechanisms given in chapter seven, may only be applied to boundary layers within this narrow range of yaw angles where the flow behaves essentially in the manner of an attached boundary layer.

4.3 Summary of Results

The flow regime where a thick turbulent axisymmetric boundary layer is formed on a cylinder in axial flow, and where transverse curvature effects are greatest, has been identified as that associated with the combination of large x/a and small Re_a, which results in large δ/a and small a^+. Boundary layers within this regime with x/a = 6000 and $300 < Re_a < 600$, producing $22 < a^+ < 41$ and $30 < \delta/a < 40$, have been selected for further study of the divergence of the characteristics of the cylinder boundary layer from those of the flat-plate boundary layer.

The experimental results for flows within the chosen regime, particularly those for mean-velocity distributions, show clearly that, in relation to a flat-plate boundary layer, transverse curvature of this order has a pronounced effect on both the inner-layer and outer-layer flow characteristics. The integral length scale θ_2 (equation [4.11]) is identified as the most appropriate outer-region length scale for axisymmetric boundary layers. However, at the same time, a momentum thickness θ evaluated by the standard flat-plate expression (equation [4.23]) is an adequate integral scaling parameter, at least over a limited Reynolds-number range, and has the advantage of being significantly less sensitive to small experimental errors in velocity measurement at the outer edge of the boundary layer. Velocity-profile similarity based on either integral length scale extends over the whole of the outer layer and into the inner layer down to $y/\theta_2 = 0.015$ ($y/\theta = 0.05$). Velocity profiles in terms of wall scales show a gradual divergence from the flat-plate case as δ/a increases and a^+ decreases, although, even at large δ/a and small a^+, the profiles always remain similar to the flat-plate profile in the innermost regions of the boundary layer (typically $y^+ \leq 10$).

The statistical analysis of the turbulence-velocity fluctuations has demonstrated a divergence from the flat-plate case characterised by the repeated, irregular occurrence of large negative fluctuations. These negative fluctuations may be associated with a turbulence mechanism which distinguishes the boundary layers examined here from flat-plate layers; they are examined further in chapter seven. As the results presented in this chapter demonstrate very little variation with Reynolds number of the distribution of mean velocity, turbulence intensity, skewness and flatness factor in the boundary layer, within the range of experiment, these further investigations have been conducted at a single Reynolds number.

Measurements for small angles of yaw have demonstrated the extreme sensitivity of the outer boundary-layer flow to yaw, confirming the need for precision in cylinder alignment to produce genuinely axial flow, and limiting the description of the axisymmetric flow processes developed here to precisely axial flow. The inner layer is less sensitive to yaw, suggesting that the inner layer is dominated by the presence of the wall. The results of further investigation of the vortex wake formed at larger yaw angles are presented in chapters five and six.

5. EXPERIMENTAL INVESTIGATION OF THE VORTEX-SHEDDING FREQUENCY

In general, at yaw angles greater than a few degrees, the asymmetry of the boundary layer increases to a point at which the flow around the cylinder shows some similarity to that of a cylinder normal to the free stream. There is a thin attached boundary layer on the windward side of the cylinder, and the flow separates to form a wake on the lee side. At small yaw angles this separated flow may form into either regular coherent vortices or a random turbulent wake in a manner similar to that of cylinders normal to the flow.

The regimes of regular vortex shedding and of random turbulence within the wake have been investigated, with the aim of establishing the boundary of the regular vortex shedding regime for small yaw angles in terms of the flow Reynolds number and the cylinder yaw angle. The regular vortex-shedding frequencies within this regime have been examined in order to establish the influence of the cylinder geometry and the flow properties on them.

The measurements of the velocity fluctuations within the cylinder wake have been made for cylinders with an l/d as large as possible (>3000) with the aim of minimising the influence of the cylinder end conditions. Care was also taken to ensure that the cylinder was not vibrating. The vortex shedding frequencies were then obtained by spectral analysis of the velocity fluctuations.

5.1 The Measurement of the Vortex-shedding Frequency

The current investigation of the flow about cylinders at small angles of yaw has identified a region of flow, at small Reynolds number, where regular vortex shedding occurs. To the knowledge of the author, this region of vortex shedding has not been investigated previously. The earlier investigations of vortex shedding from yawed cylinders have been limited to larger yaw angles ($\beta > 15°$), and previous investigations of the boundary layers formed on cylinders at small angles of yaw have been limited to larger Reynolds numbers, as on an aircraft fuselage, where no vortex shedding is observed.

The experiments were carried out in the 3-metre-long test section of the low speed wind tunnel, initially with parallel side walls with a consequent velocity increase and pressure change along the section. A new adjustable test section was designed and constructed as part of this investigation to maintain a uniform velocity. Cylinders were mounted in tension centrally within the test section, and yawed in the horizontal plane. The streamwise velocity perturbations were detected by a TSI IFA-300 constant temperature hot-wire anemometer, with a 5-μm-diameter tungsten hot-wire probe. The vortex-shedding frequencies were determined (from 64 records, with 640 samples per record) by Fast Fourier Transform of the digitised anemometer output via a Hewlett-Packard HP 3582A spectrum analyser.

Initial experiments were conducted with a 0.9-mm-diameter cylinder normal to the flow, ($\beta = 90°$) to determine a suitable probe location where the shedding frequency from only one side of the cylinder could be detected.

Measurements with the probe in the plane of yaw of the cylinder produced frequency spectra dominated by the double frequency resulting from the alternate shedding from opposite sides of the cylinder, but even slight displacements of the probe out of the plane of yaw resulted in domination of the frequency spectra by the single frequency associated with vortex shedding from one side only of the cylinder.

Displacements of the hot-wire probe by a distance y of one cylinder-diameter above the horizontal plane of yaw and approximately 3 diameters (in the plane of yaw) perpendicular to the cylinder axis were selected for further experiments with yawed cylinders, in order to maximise the signal strength of the single-frequency velocity perturbation. This optimal location of the probe is shown in figure [5.1]. The sensor of the probe was aligned horizontally, parallel to the yaw plane. The effect of vertical displacement of the hot-wire probe above the yaw plane on the velocity perturbation signal, and the resultant effects on the frequency spectra are shown diagrammatically in Figure [5.2]

Previous investigations of yawed-cylinder vortex shedding (Van Atta 1968, Ramberg 1983) have identified a mechanism where the vortex-shedding frequency "locks on" to the natural vibrational frequency of the test cylinder. In the present investigation this mechanism has been overcome by adjusting the natural frequency of vibration of the cylinder to be remote from the forcing frequency of the vortex shedding by slight increases in the cylinder tension. This allowed unequivocal measurement of the vortex-shedding frequency from the stationary cylinder. The occurrence of this "lock-on" mechanism was detected by observation of characteristic features of the vortex shedding spectra.

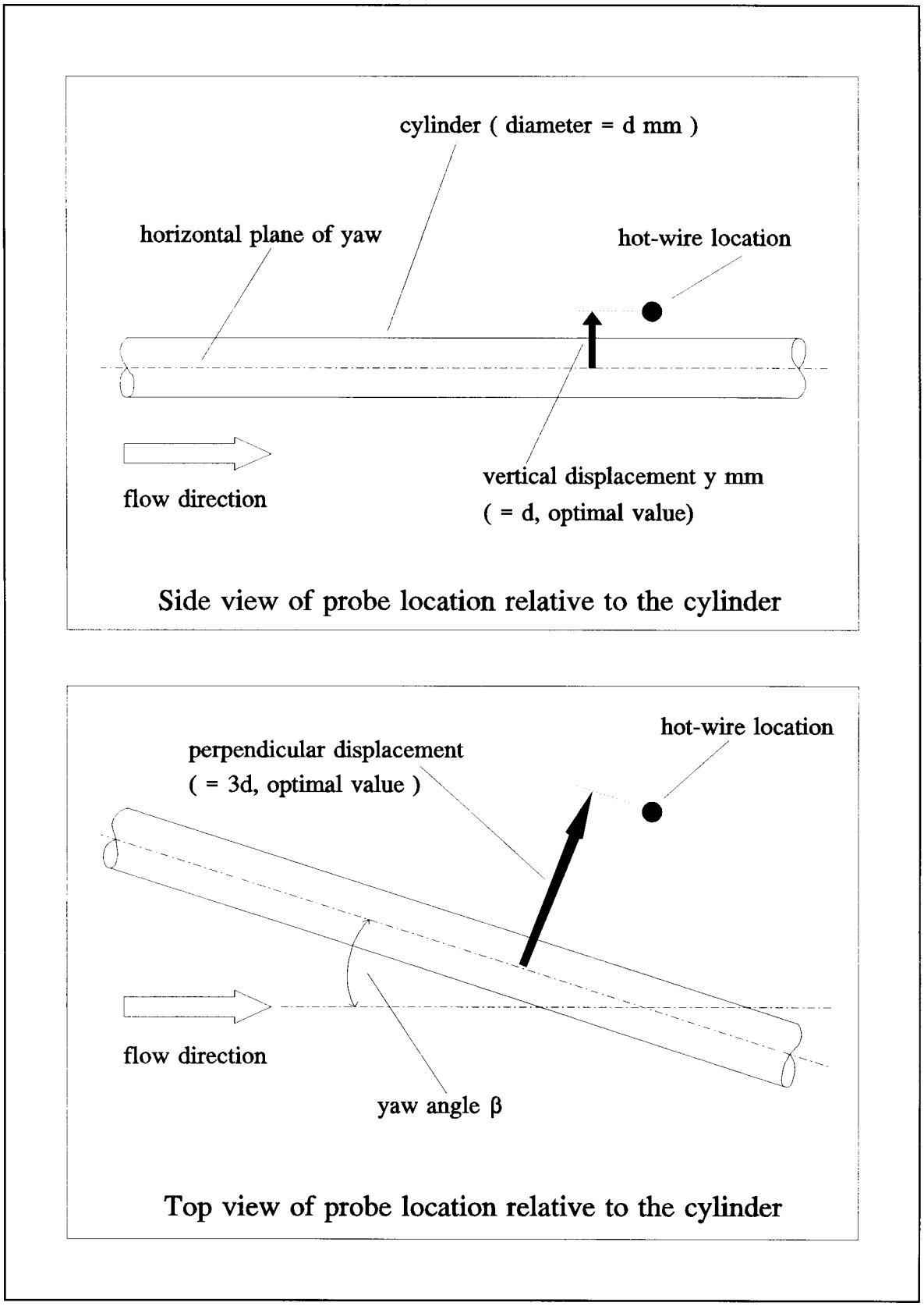

Figure 5.1 Location of the hot-wire sensor relative to the cylinder.

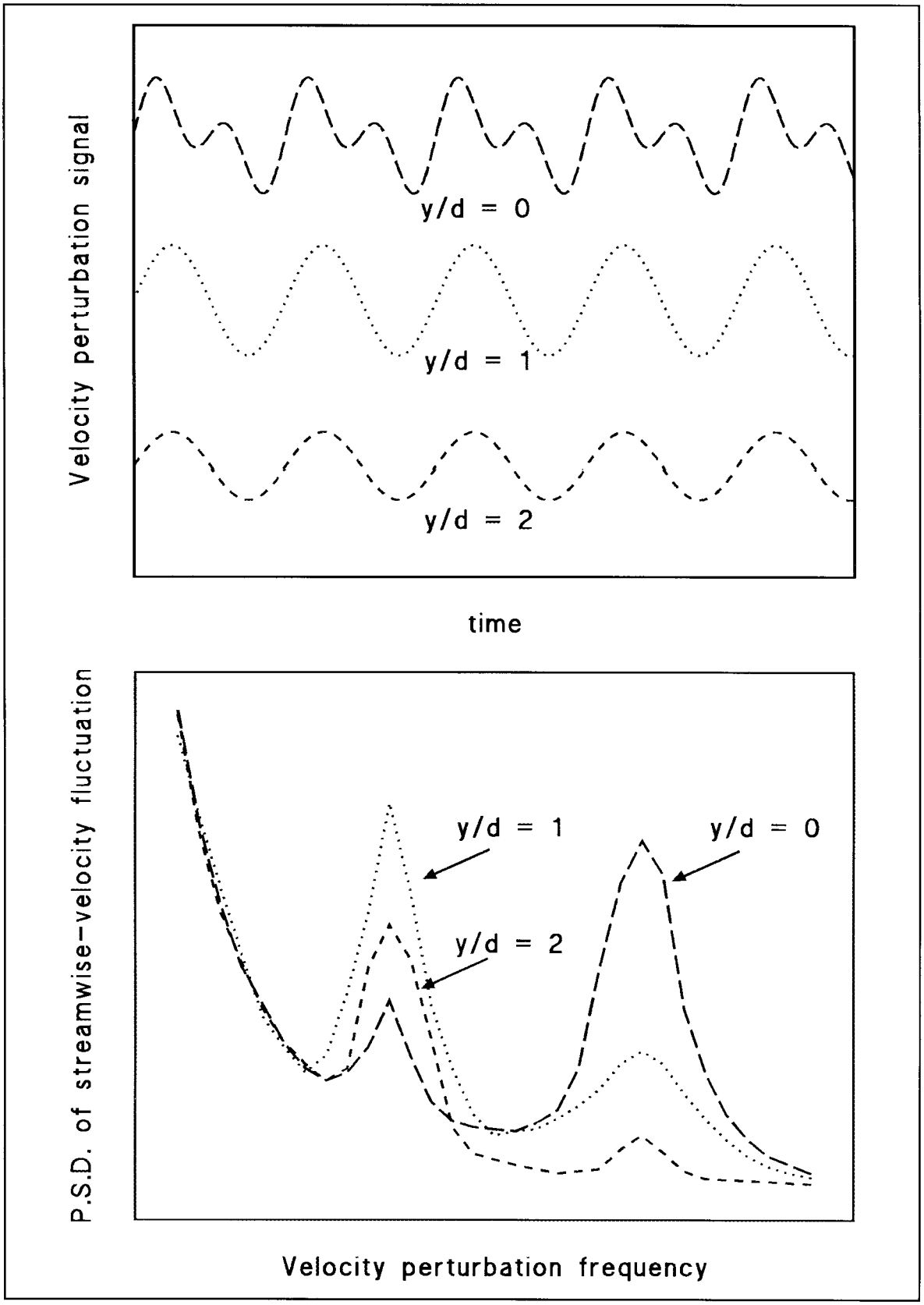

Figure 5.2 Diagrammatic representation of the velocity perturbation signal for different probe displacement y/d (upper), and the resulting vortex-shedding frequency spectra.

When natural vibration lock-on occurs, the cylinder continues to shed vortices at a similar frequency to that of a stationary cylinder, but the frequency is fixed within a very narrow bandwidth and is constant along the length of the cylinder. For experiments conducted in the variable width test section with constant velocity along the section, the occurrence of lock-on was detected by a characteristic narrowing of the single frequency peak in the velocity perturbation spectrum, shown diagrammatically in Figure [5.3].

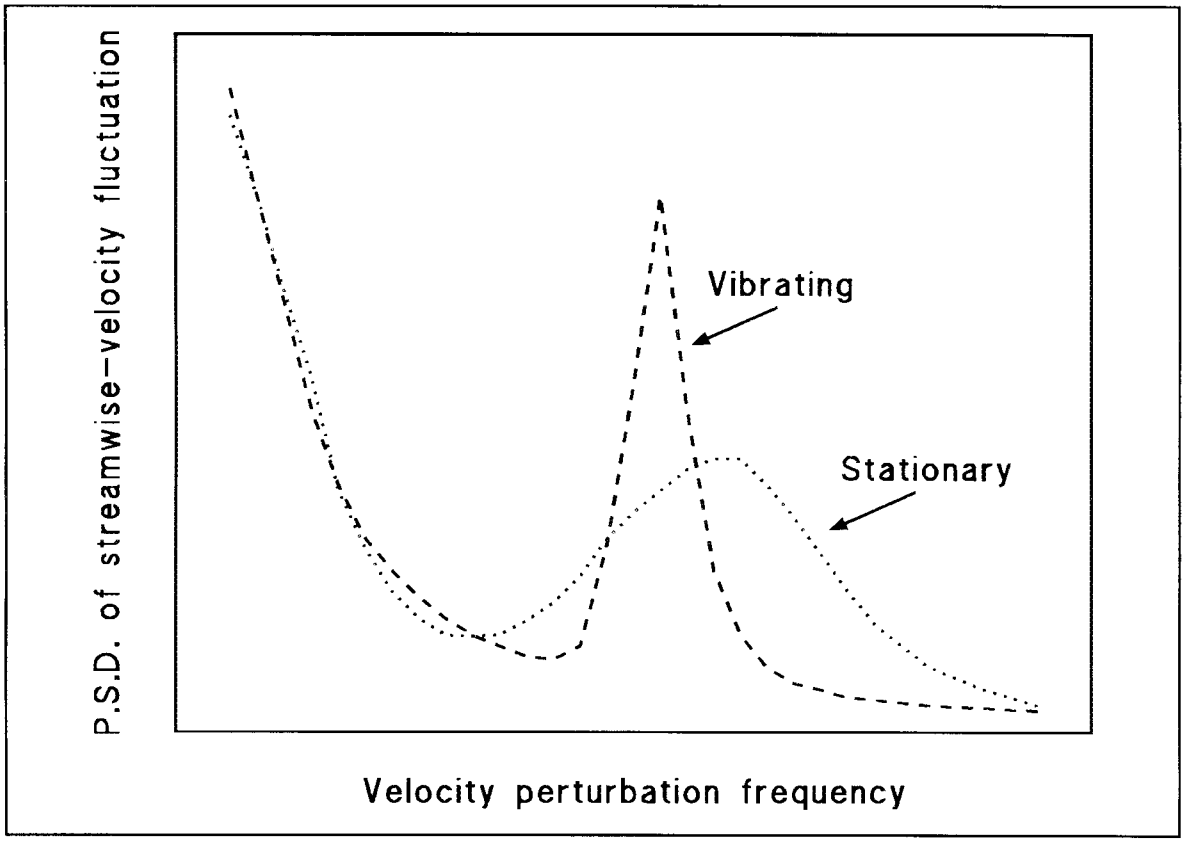

Figure 5.3 Diagrammatic representation of the velocity perturbation spectra for both stationary and vibrating cylinders in a uniform free-stream velocity at small yaw angles and small Re_a.

Experiments conducted with parallel test-section side-walls (Bull and Dekkers,1989, Appendix 1) indicated that the vortex-shedding frequency varies with the local free-stream velocity, which increases along the test section length owing to the

blockage caused by the growth of boundary layers on the walls. Simultaneous measurement of the velocity perturbation at two different streamwise locations, and thus at slightly different local free-stream velocity, produces velocity perturbation spectra with peaks at different frequencies for a stationary cylinder, and at a single frequency when the vortex-shedding frequency locks on to the natural frequency of vibration. This test allows lock-on to be detected, as shown diagrammatically in Figure [5.4].

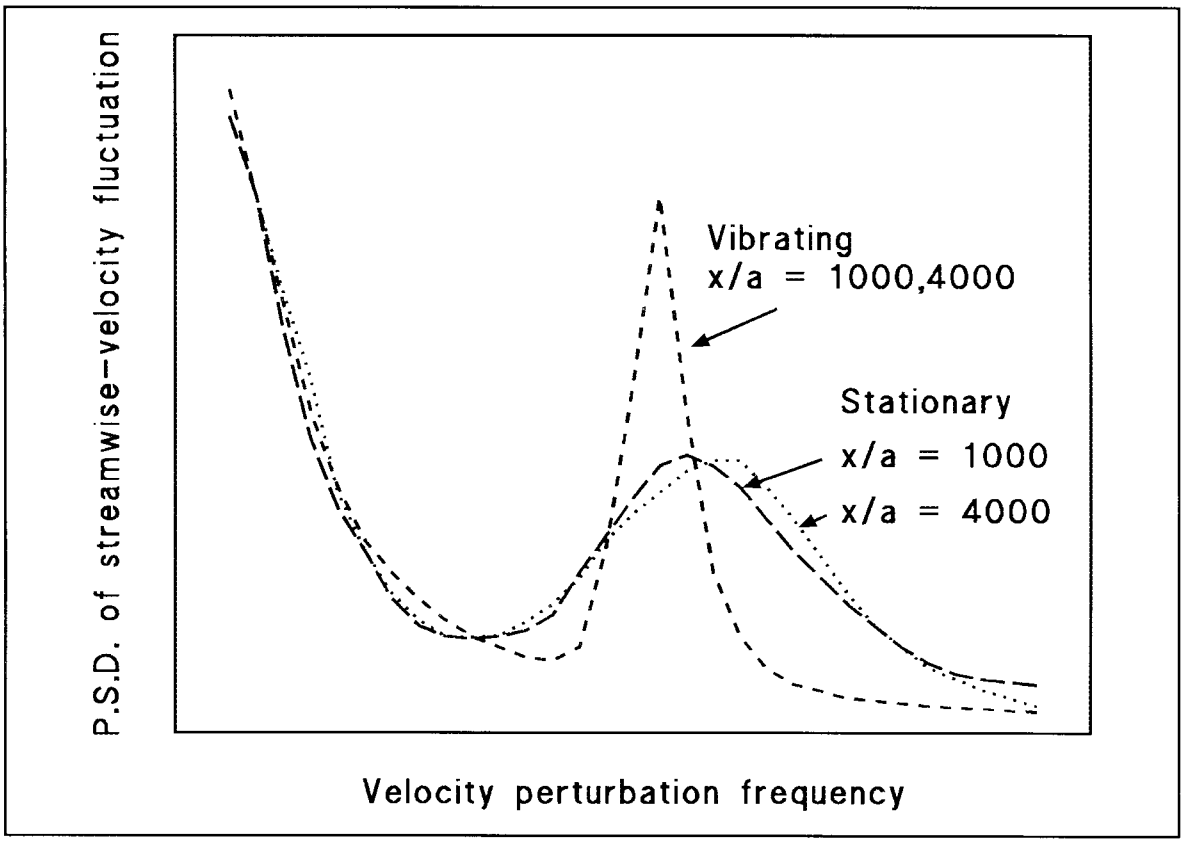

Figure 5.4 Diagrammatic representation of the velocity perturbation spectra for both stationary and vibrating cylinders at different x/a in a rectangular test section for small β and small Re_a.

An additional effect of a velocity gradient along the test section length is that the change in vortex-shedding frequency along the cylinder appears to occur in cells of constant frequency, with abrupt changes in frequency between adjoining cells. The locations of the cell boundaries along the cylinder were observed to vary with time.

These effects have also been observed by Gaster (1969) for slender cones normal to the flow , and for cylinders normal to the flow in the presence of a velocity gradient across the flow (Gaster, 1971).

When a cell boundary occurs at the probe position, the measured frequency oscillates with time between the two different cell frequencies as the cell boundary moves back and forth past the probe. The characteristic double peak of the velocity-perturbation spectrum is shown diagrammatically in Figure [5.5]. Observation of the corresponding velocity perturbation signal on an oscilloscope did not indicate any difference, other than the change in frequency, between the signal obtained at a cell boundary and the signal obtained within a single-frequency cell.

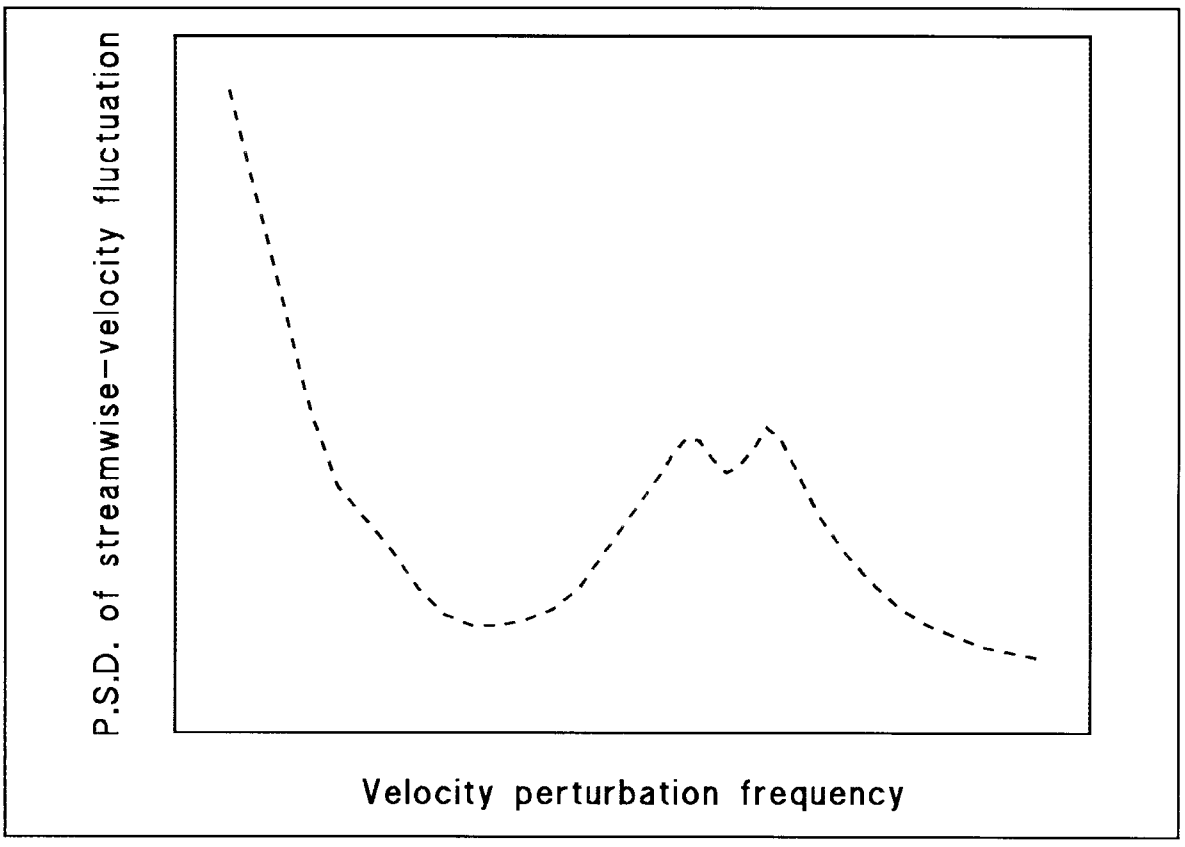

Figure 5.5 Diagrammatic representation of the velocity-perturbation spectrum obtained for vortex shedding from a yawed cylinder in a test section with a streamwise velocity-gradient, when a vortex-cell boundary occurs at the measuring probe position.

Previous investigations of vortex shedding from cylinders normal to the flow have identified end effects as a primary cause of discrepancy between results obtained in different facilities (Berger and Wille 1972, Bearman and Graham 1980). To define a more universal relationship between the Strouhal number of vortex shedding and the cylinder Reynolds number, Williamson (1988) obtained a correlation of data for various end conditions by dividing the Strouhal number by the cosine of the observed shedding angle between the cylinder and vortex axes. This implies that suitable end conditions are those which produce parallel shedding for cylinders normal to the flow.

As there is no expectation that parallel shedding should occur for the yawed cylinders in the present study, in which end effects are absent, no attempt has been made to manipulate the cylinder end conditions as there is no quantitative outcome from which to determine when the correct end conditions have been applied. The best that can be done is to use cylinders with as large an l/d as possible. In the present work all cylinders tested had $l/d > 3000$.

To maintain a consistent upstream end condition, the upstream end of the test cylinder was always located at the start of the test section, because experiments with the cylinder extending upstream into the wind-tunnel contraction indicated that the cellular vortex pattern arising from the changing velocity within the contraction extended into the test section and affected the vortex-shedding frequency.

5.2 The Regime of Regular Vortex Shedding

The results from the present investigation extend the range of yaw angles for which vortex-shedding frequencies have been measured from its previous minimum in the region of 15°, down to angles in the region of 1°.

The Reynolds number range for which vortex shedding occurs for cylinders normal to the flow ($\beta = 90°$) is well established, with two regions of vortex shedding as defined by Roshko (1954). The first region of regular vortex shedding occurs for $40 < Re_d < 150$, where laminar shear-layers separate from the cylinder and form "viscous" vortices which move downstream in a "vortex street". [It should be noted that published work in which cylinders normal to the flow are taken as a reference point makes use of Reynolds numbers Re_d based on cylinder diameter, rather than the Reynolds number Re_a based on cylinder radius which has customarily been used for axial flow investigations]. A second region, of irregular vortex shedding, occurs for $Re_d > 300$ where the shear layers undergo laminar-turbulent transition as they separate from the cylinder surface. These separated shear-layers then form periodic turbulent vortices within a turbulent wake. The coherent vortices finally diffuse into the background turbulence downstream. These two regions are separated by an unstable transition range, $150 < Re_d < 300$, where laminar-turbulent transition occurs within the shear layers after separation but before the formation of the (then) turbulent vortices. The lack of a fixed position for the transition process leads to fluctuations in the frequency of vortex formation within this range.

The Reynolds number limits for regular vortex shedding from cylinders at small

yaw angles $\beta°$ have been investigated here for a range of cylinder diameters and yaw angles by varying the mean flow velocity while observing both the velocity perturbation signal and the derived frequency spectra. The results presented (which are an extension of those given by Bull and Dekkers, 1989, and 1993a - reproduced as Appendices 1 and 4 respectively) were obtained with wind-tunnel side-walls adjusted to produce zero streamwise pressure-gradient.

Both the maximum velocity at which the velocity perturbation signal still appears free of irregularities, and the maximum velocity at which the vortex-shedding frequency is still discernible from the background turbulence in the velocity-perturbation spectrum, have been recorded. Characteristic velocity-perturbation signals and the corresponding frequency spectra are shown diagrammatically in Figure [5.6] for regular vortex shedding, for the onset of irregularities in the signal, and for the disappearance of the vortex-shedding frequency peak into the background turbulence within the frequency spectrum. Experiments were conducted with cylinders of diameter 0.90, 1.93 and 2.95 mm for yaw angles $1° < \beta < 10°$ over a mean flow velocity range of 2 to 27 m/s, corresponding to a Reynolds number range of $60 < Re_a < 2700$ ($120 < Re_d < 5{,}400$).

No lower Reynolds number limit for vortex shedding was detected, suggesting that, if one exists, it corresponds to a flow speed below the minimum stable flow speed of the wind tunnel, even for the smallest diameter cylinder tested here.

As for cylinders normal to the flow, there is no upper Reynolds number limit above which vortex shedding does not occur, but rather a boundary below which regular vortex shedding is detectable. The upper Reynolds-number boundaries

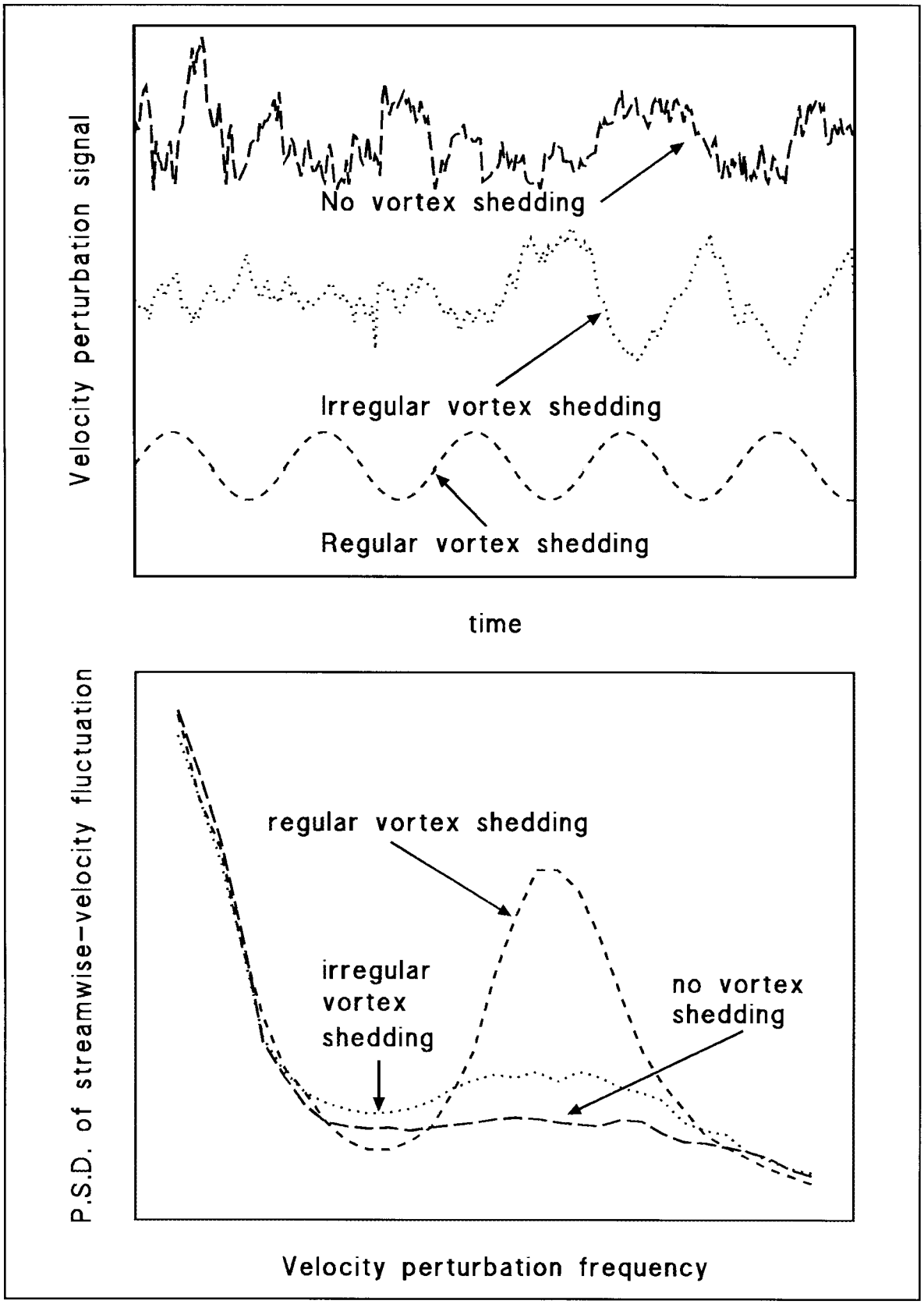

Figure 5.6 Diagrammatic representation of the velocity perturbation signals and frequency spectra typical of the three Reynolds number regimes.

determined here for both regular vortex shedding, and detectable irregular but continuous turbulent vortex shedding, are shown in Figure [5.7]. Whether the limit for regular vortex shedding corresponds to the Re_d = 150 (Re_a = 75) limit for cylinders normal to the flow is as yet unknown. Further extensive experimentation examining the laminar-turbulent transition processes in the separating shear layers of yawed cylinders is required to obtain a better understanding of the Reynolds-number limits for the different flow regimes which may occur in the wake of yawed cylinders. Figure [5.7] shows only results for yaw angles $\beta > 1°$; at smaller angles still, down to 0.5°, continuous but somewhat irregular vortex shedding was detectable, and at angles less than 0.5° intermittent bursts of irregular vortex shedding were observed.

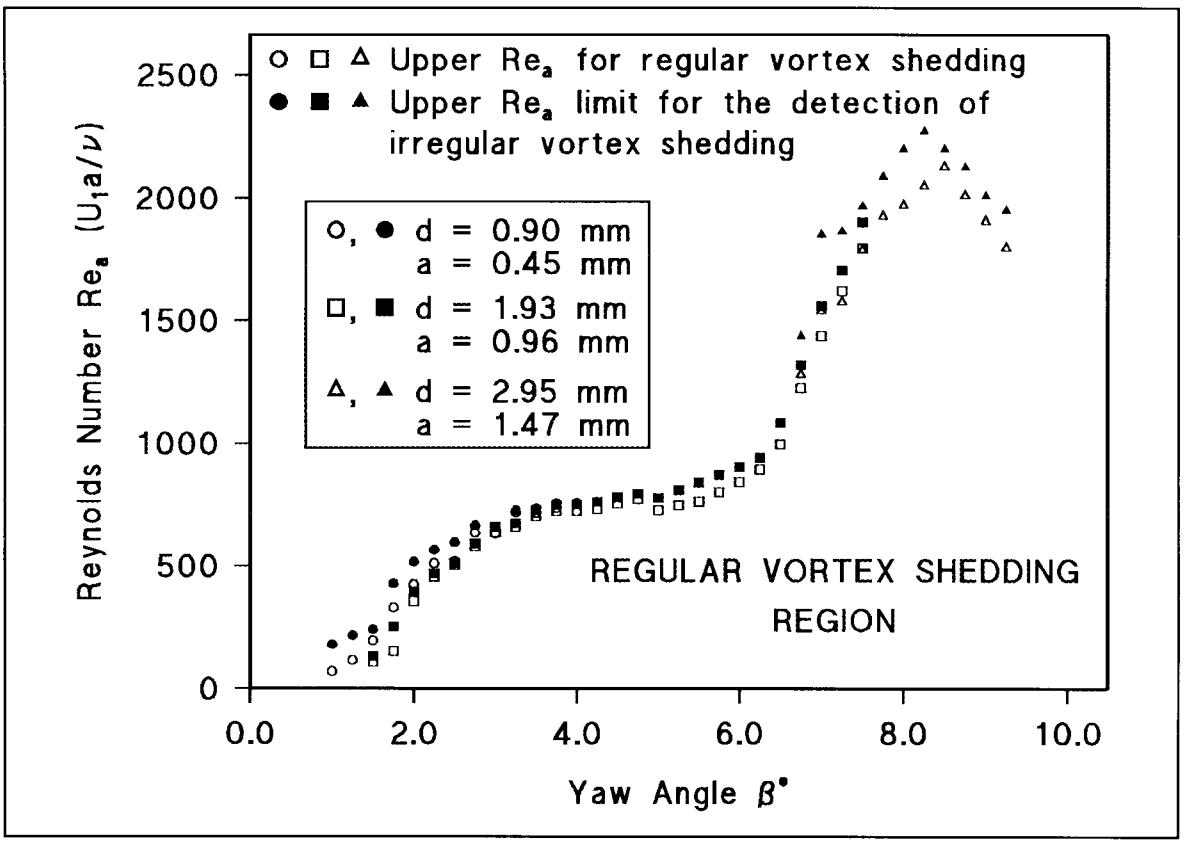

Figure 5.7 The region of vortex shedding observed for cylinders at small angles of yaw, showing the upper Reynolds number (Re_a) boundaries for both regular vortex shedding and detectable irregular but continuous (turbulent) vortex shedding.

It might also be noted that the results for zero pressure-gradient shown in figures [5.7] and [5.8] and the corresponding results for flow with mild streamwise pressure-gradient associated with the parallel-sided wind-tunnel test-section (Bull and Dekkers, 1989, Appendix 1) are very closely similar.

The flow regime boundaries determined for Re_a may also be expressed in terms of a Reynolds number Re_n based on the normal velocity component, as shown in Figure [5.8]. The observation that the upper limiting value of Re_n is not constant at a value of 150, and that the lower limiting value of Re_n, if one exists, is below 40 is further evidence that the independence principle has little relevance at the small angles of yaw examined here.

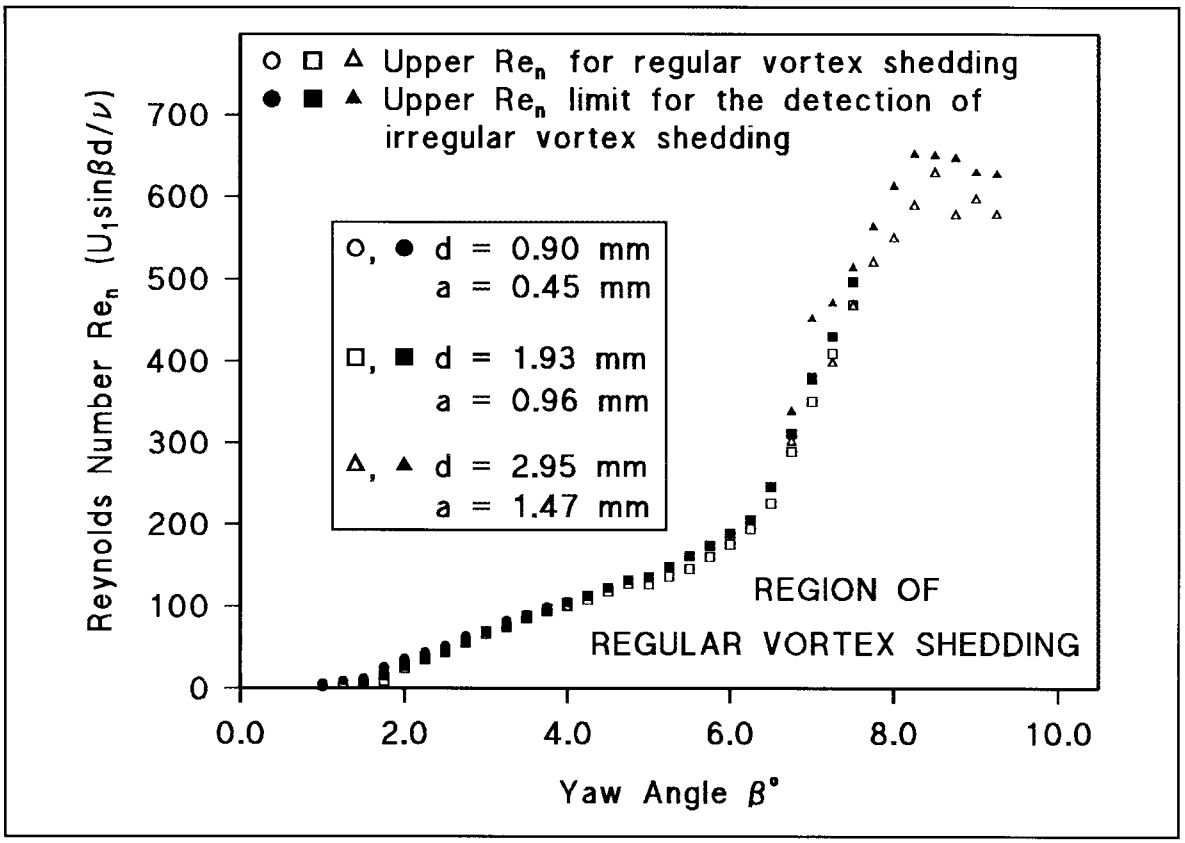

Figure 5.8 The region of vortex shedding observed for cylinders at small angles of yaw in terms of the Reynolds number Re_n ($= 2Re_a\sin\beta$) based on the component of the free-stream flow normal to the cylinder axis.

5.3 The Frequency of Vortex Shedding

The frequency of vortex shedding has been measured for cylinder yaw angles spanning the gap between axial flow and the previously reported yawed cylinder data. To facilitate incorporation of the new measurements into the existing data, measurements were made at constant values of Re_n, the Reynolds number based on cylinder diameter and the component of the free stream velocity normal to the cylinder axis. The vortex shedding frequency has been expressed in non-dimensional form both as a frequency parameter $F = fd^2/\nu$, and as a Strouhal number $St = fd/U_1$.

The Strouhal number is the preferred form for comparison of the present results with previously published data in which it is the most common form of non-dimensional frequency. The frequency parameter is the preferred form of non-dimensional frequency for examination of the relationship between flow velocity and vortex-shedding frequency, as this allows these two dimensional parameters to be separated, whereas they are both included in the Strouhal number $St = F/Re_d$. The closely linear relationship between F and Re_d found for cylinders normal to the flow at small Reynolds numbers, which produces an almost constant Strouhal number, provides a useful reference for the frequency / velocity relationship for yawed cylinders at similar small Reynolds numbers.

In the early part of the present work, vortex-shedding frequencies were measured in the wind-tunnel test-section with parallel side walls and therefore mild streamwise pressure gradient (Bull and Dekkers,1989, Appendix 1). The variation of

frequency parameter with yaw angle and Reynolds number is similar to that subsequently found for flow with zero pressure-gradient. Previously, no distinction was made between the results for the two cases (Bull and Dekkers 1993a, Appendix 4). However, closer examination of the data shows that there are noticeable differences: the frequencies for non-zero pressure-gradient are somewhat higher for $\beta \leq 6°$, but somewhat lower for $\beta \geq 6°$. A comparison of results from the two types of flow, for $\beta = 2°$, $6°$ and $10°$, is shown in Figure [5.9]. The differences are attributed to the pressure-gradient associated with streamwise variation of the free-stream velocity resulting from growth of the boundary layers on the side walls of the test section. Here, only the data for flow with zero pressure-gradient are considered further.

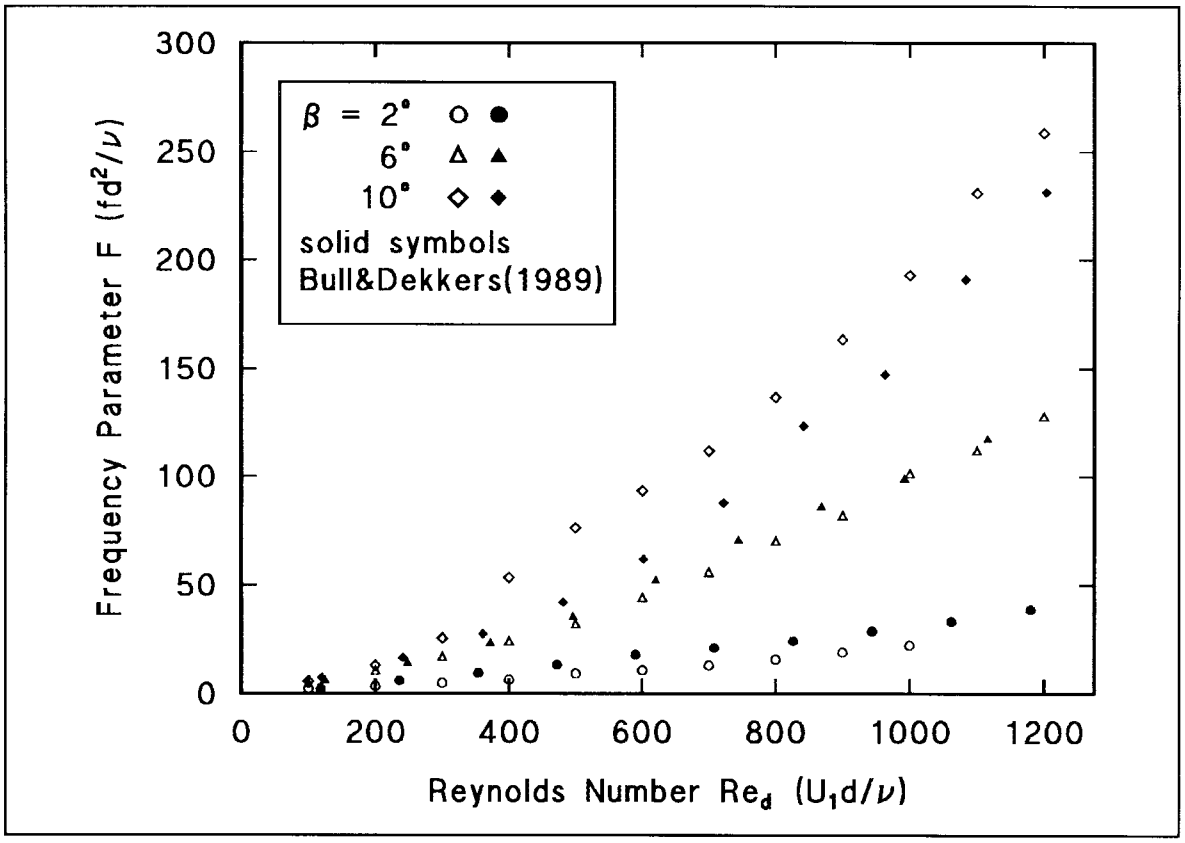

Figure 5.9 Variation of Frequency parameter F with Reynolds number Re_d for constant yaw angles spanning the range of investigation, d = 0.9 mm, with zero pressure gradient, and similar data with a streamwise pressure gradient.

The measurement of vortex-shedding frequency for two different cylinder diameters (d = 0.9 mm and d = 1.93 mm), at constant values of the Reynolds number Re_n based on diameter and the normal velocity component, are shown in Figure [5.10]. This figure shows the variation with cylinder yaw angle β of both the frequency parameter and Strouhal number.

Yaw angles greater than $\beta = 12°$ were produced by passing the downstream end of the test cylinder out through a small hole in the side wall of the wind-tunnel test-section, allowing the upstream end condition to remain the same for all the measurements. The variation in the downstream end condition was unavoidable for the larger angles, and any effect on the vortex-shedding behaviour may be expected to be less significant than the alternative of varying the upstream support.

Whether the vortex shedding frequency is non-dimensionalised as frequency parameter or Strouhal number, the results shown in Figure [5.10] indicate that there is no systematic effect of cylinder diameter on vortex shedding behaviour: either form of non-dimensionalisation adequately accounts for the effects of varying cylinder diameter.

The addition of the present data to the range of previously published data at larger yaw angles is shown in Figure [5.11] as the variation of Strouhal number with yaw angle for constant Re_n of 50, 80 and 150 for the complete range of possible yaw angles from $\beta = 0°$ (axial flow) to $\beta = 90°$ (cylinder normal to the flow). The present results follow on smoothly from the previous results by Van Atta (1968) for cylinder diameters of 0.79 mm and 1.14 mm, and yaw angles from 90° down to 15°.

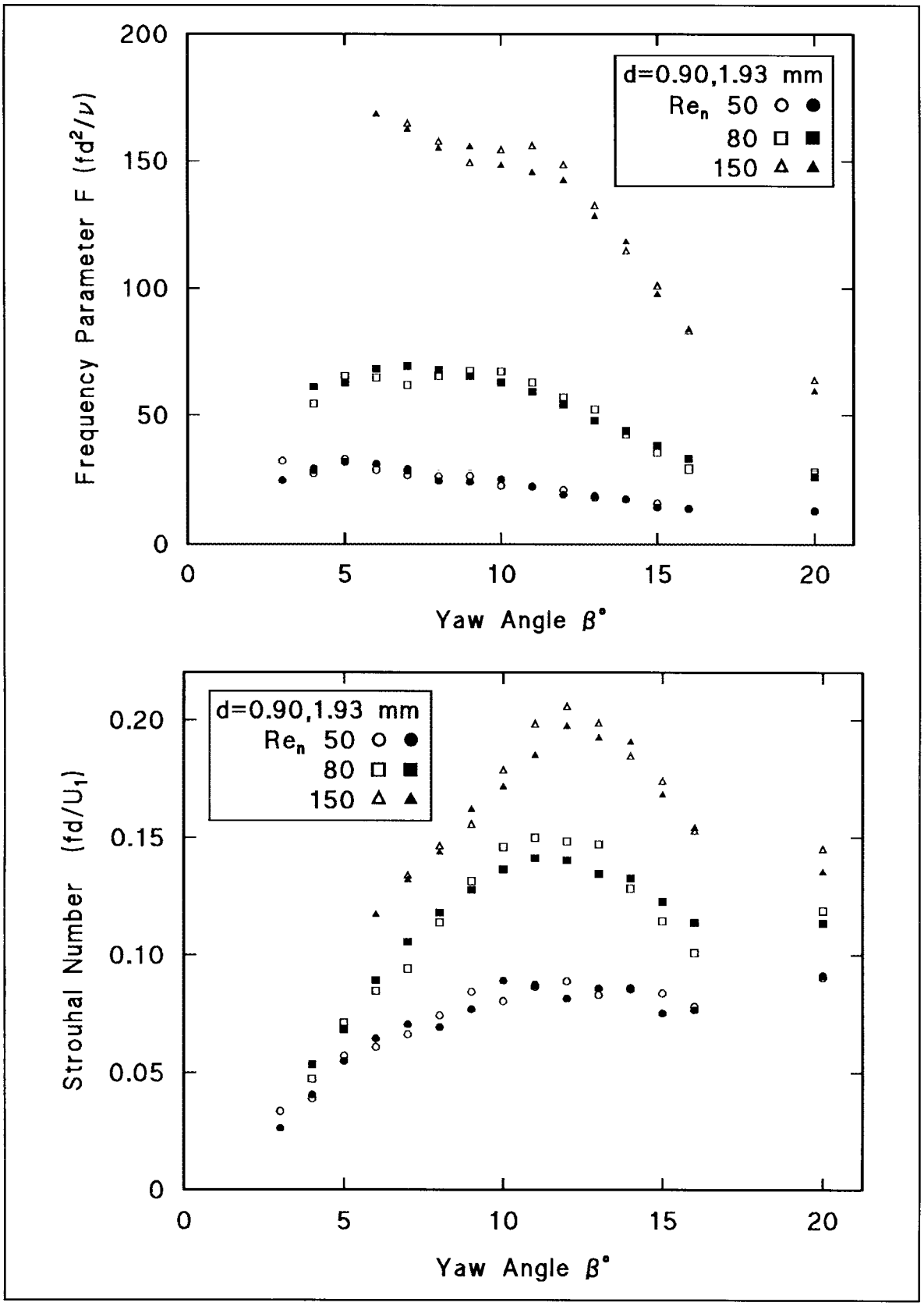

Figure 5.10 The variation of Frequency parameter F and Strouhal number with cylinder yaw angle $\beta°$ for constant Reynolds number Re_n (= $2Re_a\sin\beta$) and cylinder diameter d.

Although the present results match smoothly with the previously published data for larger yaw angles, the behaviour of the Strouhal number at smaller yaw angles is seen to become far more complex than that observed at larger angles for constant values of Re_n. Because the axial component of the free stream velocity becomes increasingly significant as the yaw angle decreases, the use of the normal velocity component as the characteristic velocity in the Reynolds number is seen to become increasingly inappropriate as the yaw angle decreases. The inclusion of the velocity in the Strouhal number also adds to the complexity of these results.

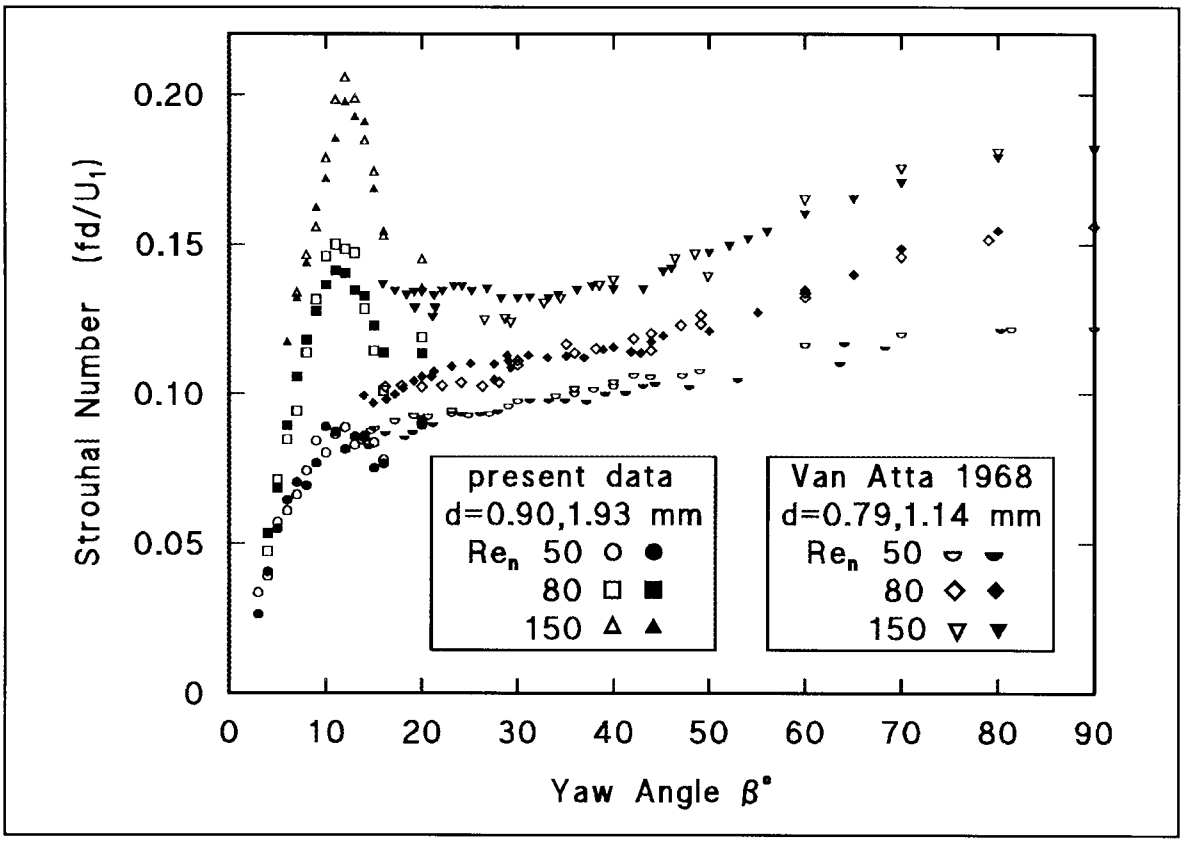

Figure 5.11 The variation of Strouhal number with cylinder yaw angle $\beta°$ for constant Reynolds number Re_n ($=2Re_a\sin\beta$), with previous results by Van Atta (1968) at larger yaw angles, for different cylinder diameters d.

As both the present results and the previous results by Van Atta (1968) indicate that physical similarity of the flow extends across a range of cylinder diameters, further experiments were confined to a single cylinder diameter of 0.9 mm. Frequency measurements were made for a range of velocities corresponding to set values of Reynolds number Re_d for each yaw angle up to $\beta = 12°$.

The measured frequencies are shown in Figure [5.12], for large yaw angles, and Figure [5.13] for small yaw angles, in terms of both Strouhal number and frequency parameter. Again, the separation of the velocity and the frequency terms in the upper graphs, where the frequency parameter is used, appears to reduce the complexity of the variation of non-dimensional frequency with Reynolds number.

The approximately linear relationship between F and Re_d observed for cylinders normal to the flow is also apparent for each yaw-angle data set shown in Figures [5.12 and 5.13]. For each yaw angle non-linearity in the relationship is greatest at the smaller Reynolds numbers, suggesting that the free stream velocity is not the characteristic velocity of the flow at yaw angles other than 90°.

The increase in the slope of the F-Re_d relationship with increasing yaw angle shown in Figures [5.12] and [5.13] suggests that the characteristic velocity of the vortex-shedding mechanism increases with yaw angle for a fixed free-stream velocity. This variation of the characteristic velocity with the cylinder yaw angle appears to be more complex than simply the increase in the magnitude of the normal velocity component $U_1 \sin\beta$, but at larger yaw angles ($\beta > 45°$) the normal velocity appears to be the dominant factor in the characteristic velocity.

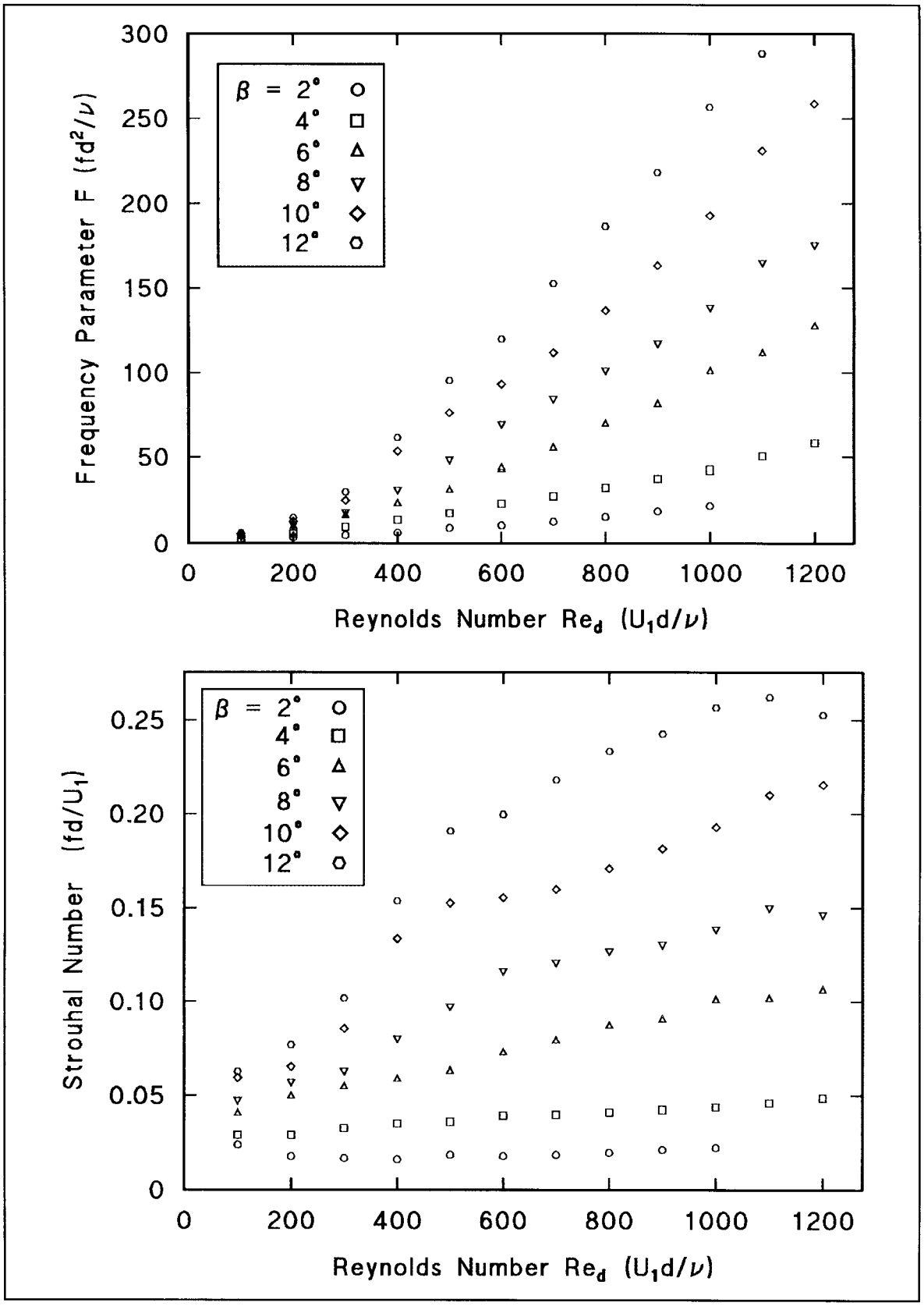

Figure 5.12 Variation of Frequency Parameter F and Strouhal number with Reynolds number Re_d for constant yaw angles spanning the range of investigation, d = 0.9 mm.

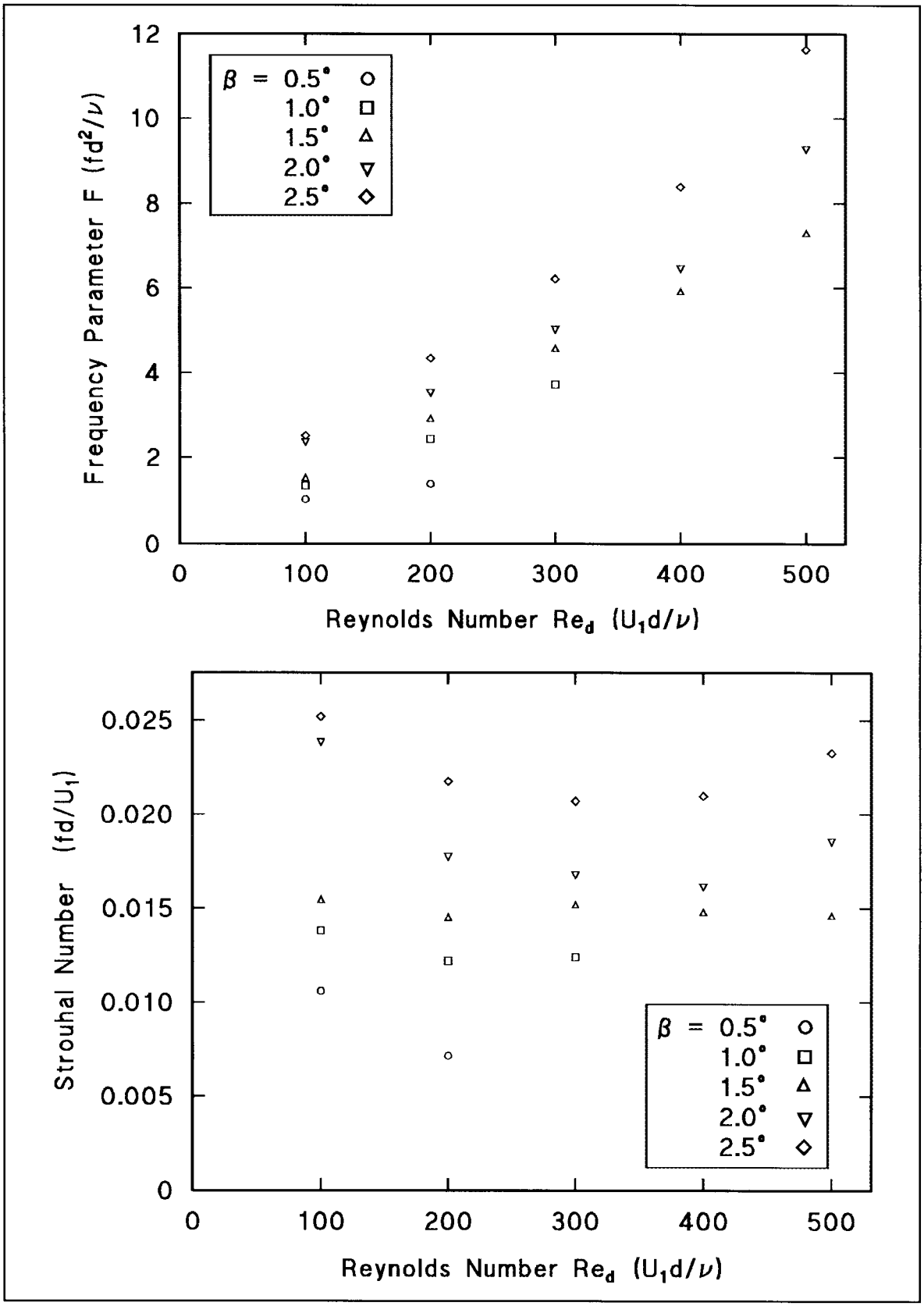

Figure 5.13 The variation of Frequency parameter F and Strouhal number with Reynolds number Re_d for very small angles of yaw, $\beta°$ less than 3°, for d = 0.90 mm.

Further insight into the controlling factors of the vortex shedding frequency is obtained by cross-plotting the frequency data against the yaw angle at constant values of Reynolds number, as shown in Figure [5.14] for both frequency parameter and Strouhal number.

Again the Frequency parameter provides the less complex picture of the relationship between frequency, yaw angle and Reynolds number. For each Reynolds number, the frequency increases almost linearly with yaw angle for the small range of angles considered here. It might be noted that dependence of frequency on the normal velocity component $U_1 \sin\beta$ would also appear as linearity at small yaw angles.

A simple empirical relationship between the vortex-shedding frequency and yaw angle (in radians) was obtained by Bull and Dekkers (1989, Appendix 1) from the non-zero-pressure-gradient data in the form

$$F = A\ \beta^n, \qquad [5.1]$$

where A and n are both functions of Reynolds number, given by

$$A = 28 + 782(Re_d/1000)^{2.66} \qquad [5.2]$$

and

$$n = 0.46 + 0.483(Re_d/1000)^{1.06}. \qquad [5.3]$$

Equations [5.1] to [5.3] do not carry over particularly well to flow with zero pressure-gradient. A similar relation for zero-pressure-gradient flow could be obtained

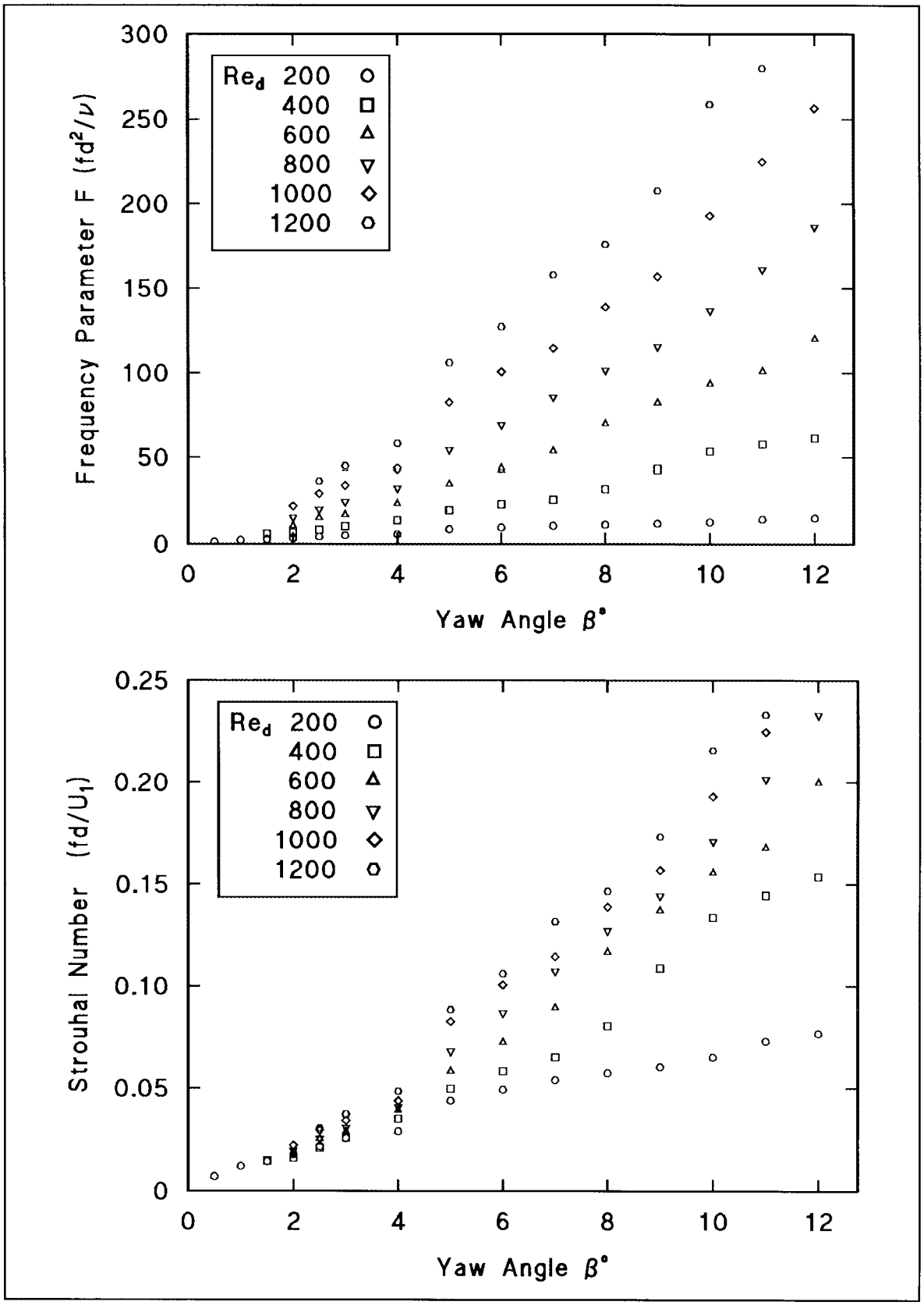

Figure 5.14 The variation of Frequency parameter F and Strouhal number with the cylinder yaw angle β for constant Reynolds number Re_d, for d = 0.90 mm.

from the data of Figure [5.14], but this has not been done: an alternative analysis of the dependence of frequency on Reynolds number and yaw-angle, based on the results of flow visualisation experiments is given in the next chapter.

Equations [5.1] - [5.3] and similar equations for zero pressure-gradient are valid for cylinders at small yaw angles; such estimations of the frequencies which may be expected in the cylinder wake are of considerable interest to researchers engaged in distinguishing fluid-generated noise from the background sounds detected by towed sonar arrays. Alternative forms of Equation [5.1] will be investigated in chapter six of this thesis: further study of the nature of the vortex wake behind yawed cylinders, by flow visualisation, leads to a form of Equation [5.1] which more accurately reflects the characteristic velocity associated with a yawed-flow geometry.

5.4 Summary of Results

A new flow regime of regular vortex shedding at very small yaw angles has been identified. The boundary of this regime has been determined as an upper Reynolds number limit which varies with yaw angle. The dependence of the measured vortex-shedding frequency, expressed either as frequency parameter or Strouhal number, on yaw angle and Reynolds number has been obtained. New measurements of Strouhal numbers at very small yaw angles are shown to integrate well with the existing data for larger yaw angles. Experiments were conducted with, as far as possible, minimal external influences on the wake flow resulting from the cylinder end conditions, and it was ensured that the cylinder was not vibrating for the results presented here.

The dominant parameters which influence the shedding frequency are the cylinder Reynolds number and the yaw angle. The effects on the vortex-shedding frequency of streamwise position, expressed in non dimensional form as x/a, are found to be negligible. The independence principle, the notion that the Strouhal number scales on the cross-flow velocity component only, is shown to be invalid, although there is a purely fortuitous correlation with the experimental data at larger yaw angles.

Although an empirical relationship expressing the frequency parameter as a function of the cylinder yaw angle and Reynolds number for flow with mild non-zero pressure-gradient has been formulated previously, derivation of a corresponding empirical relationship for the zero-pressure-gradient case is delayed to a later chapter.